In this document we make a point-by-point response to the reviewers remarks. We also provide the marked-up version of the submitted manuscript highlighting the changes. According with the reviewers suggestions new sections and analysis are added. The manuscript was also partially re-written.

Response to Reviewer 1

General comments:

1. It is not obvious from the paper what are the implications of your results for sea ice thickness measurements from satellite, e.g. SMOS or the upcoming CIMR mission.What is the relative importance of decimetre roughness compared to other factors? Do the current incidence angles employed by SMOS limit the sensitivity of measured Tb to roughness? I expected to see a statement on this in the abstract and some discussion later on the manuscript.

»> The discussion is now included in the manuscript: The SMOS SIT is derived from near-nadir measurements (0-30degrees) therefore the expected change in the TB due to the large scale surface roughness (up to -2.6K) is negligible compared to the uncertainty associated with other factors, such as sea ice concentration (-1.5K/%), and snow cover (8.5K/m). The effects of surface roughness are most pronounced for incidence angles >40deg and stronger on vertical polarization. We have added the statements regarding that current and future L-band missions (SMOS, SMAP, CIMR, SMOS-HR) that can be affected.

2. The airborne altimeter data provide measurements of the snow surface roughness, but this is not necessarily reflected directly in the underlying ice-snow interface roughness. There is no discussion of this in the manuscript and the potential issues/errors it could introduce. Which is most important for L-band emissivity, snow or ice surface roughness? Might the roughness be overestimated if it's the ice interface roughness that you need to know?

»> The altimeter measures the snow surface elevation but we lack snow thickness data. Therefore we have to assume that snow is plane-parallel layer to the sea ice surface. Although dry snow is transparent in L-band it has an impact on ice thermodynamics, which determine the ice effective temperature and emissivity (snow layer also refracts the radiation, but it is more relevant for higher incidence angles).

Regarding the overestimation of the sea ice roughness due to snow cover. We would rather expect the opposite effect, the underestimation of the surface roughness. Snow will cover the ragged edges of the pressure ridges and ice flows.

In the sensitivity study we calculate the model sensitivities for different assumptions about snow thickness. The importance of the snow thickness is now illustrated on two new figures: 8 and 9. The change of TB due to the snow thickness is up to 18K (from 0 to 1m) for sea ice surface temperature of 250K.

3. It is not clear whether the assumption of isotropically-oriented surface roughness features is valid, even when averaging model-data comparisons over 5 km. Is the sensitivity of modelled Tb to surface feature orientation linear? When modelling Tb over 5km, the assumption is that Tb will be the average of a uniform distribution of surface feature azimuth angles. But is it reasonable to assume the average of short radiometerTb integrations, from sea ice with lots of different surface feature orientations, is mea-suring the same thing? Is there any geometrical shadowing of facets at the 45-degree incidence angle? If so, how do you account for this in the simulations?

»> Regarding the isotropic orientation of surface facets. We now include the analysis of the surface slopes azimuthal orientation: figure3. Although the comparison with the radiometer data is not conclusive at 5km, we aim at generalizing the roughness parametrization for a larger region, so as to infer the implications for SMOS/SMAP/CIMR (resolution of 40km), at such scale it is less likely that the sea ice will have coherent ondulations on the surface. The impact of such oriented sinusoidal surfaces on the angular characteristics is discussed in Ulaby and Long (2014) in chapter 10.4., which served as an inspiration for our approach.

In the simulation the shadowing occurs when the local incidence angle is greater than 90deg, therefore radiation from such facet is emitted away from the antenna. Current version of the statistical model, with the facet orientation drawn from the CDF, does not account for the "double-bounce" reflections.

4. Could you not just use the observed empirical CDF within each 70 m footprint,rather than the statistical model fit, to simulate Tb? i.e. integrate over the N pairs of angles for each facet within the 70 m footprint.

Is this just to speed up your simulations($70^2/0.5^2$ is only about a factor 2 larger number of facets than your 10^4 criteria), or so you can calculate average model results over 5 km sections? Using the observed CDF may produce a better model fit to the radiometer observations.

»> We considered the direct assimilation of the facet orientation from the DEM but this method will be only applicable to the nadir antenna as the side-looking footprint is not scanned. In the manuscript version submitted on 2019/10/31 we use the empirical CDFs derived directly from the ALS measurements.

Another associated issue is the assumption on the ice thickness and snow thickness of each facet. Although these can be substituted with constant values for the whole footprint. Additionally, the position of the facets within the antenna gain function, which is unknown for this particular system mounted on the airplane. The assumption of the constant gain that we used in the manuscript is more accurate as the signal is averaged over a larger distance. All things considered, the assumptions that have to be made and rather small expected signal (up to 8K) directed our efforts to establish a simple robust parametrization which considers an isotropic slope orientation.

5. A particularly useful contribution of this paper would be a more in-depth model sensitivity analysis of the relative effect of roughness on measured Tb compared to other factors. The current results touch on this with e.g. Fig 6, but by keeping other factors constant in the simulations its impossible for the reader to understand the true sensitivity to roughness. For example, how different does Fig 6 look for a different set of sea ice constants? E.g. 3 m thick, fresh MYI, with thicker snow depth and a warmer surface? I would recommend removing Figs 7 and 8, which don't really contribute to the message of the paper, and adding some deeper theoretical analysis of the relative impact of roughness on L-band Tb.

»>Thank you for this suggestion, the sensitivity analysis is now included in the manuscript. Based on it we present that surface roughness has a much smaller impact on the L band TB of sea ice than snow cover. New figures: Fig 8a, b, c show the non-linear and non monotonic relation between TB and surface temperature, plotted for different snow thicknesses. Table 2. Contains the partial sensitivities to of the TB to the various inputs, for lower and higher temperature ranges as well as for set of assumptions on snow thickness. The previous figures 7, 8 are removed.

6. Results from the comparison between modelled and observed Tb are not promising and are difficult to interpret here. I had many questions looking at Figs 9 and 10 that were not discussed within the text. Based on the theoretical results in Fig 6, you'd probably only expect an improvement to the 45-degree angle v-pol channel when in-cluding the effects of roughness, right? So the poor correspondence between model and observations is likely one or more of: model inaccuracy, the model configuration(no. layers, penetration etc.) not being adequate, simple treatment of ice thermody-namics, not having altimeter observations for the 45-degree footprints, or the limited treatment of snow. Without showing results from a model sensitivity analysis of these factors though, it is impossible to interpret which factor or set of factors is most likely.Why is there such a low dynamic range for modelled Tb's in most cases where mea-sured Tb >220-240K? Can you add another figure showing the absolute differences between modelled Tb for simulations with and without GO roughness included, per-haps as histograms or as a function of the surface roughness?

»> The discussion of the comparison between modeled and measured TB is now interpreted with the sensitivity study in mind. The simple emission model used in our study (one layer of ice with one layer of snow) has much more sensitivity to the snow thickness than to the surface roughness. We added new figures showing the histogram of the differences between measurements and the simulations setups for all four antenna feeds. Overall, the simplified one-layer model poorly simulates the sea ice TB.

7. The written English needs some improvement throughout the manuscript. I would recommend a careful proof-read to check spelling and grammar. A few e.g.'s just on the first page are:

L2 'rely on', »> corrected

L8 you mean 'horizontal polarization'? »> corrected

Minor comments/edits:

Page 1. Line 7. Effect on what? What scale of roughness? Multiple scales?

»> corrected

L 18. Surface roughness of the ice or snow, or both?
»> corrected

P2 L5. Both high and low spatial frequencies. . .
»> corrected

L11. What do you mean by 'stays unnoticed'? Rephrase
»> rephrased to: the surface roughness in negligible

L18. What is 8*lambda for L-band?Intro Section. What about the other factors affecting Tb from sea ice? They are not the primary focus of this study, but can complicate your interpretations of the roughness effects, particularly when comparing model results to radiometer observations. So you should introduce the effects of e.g. thermodynamics, ice concentration, snow proper-ties etc. here. Are there any previous estimates of the impact of roughness on L-bandTbs?
»> There are a number of studies regarding effects of surface roughness on the L-band TB of soils, as this wavelength is widely used for soil moisture retrieval. To our knowledge this is the first time that the impact of surface roughness is on L band emissions from sea ice is evaluated.

P3 L8-9. What was the air temperature then? Thermodynamic effects on the snow properties may explain your difficulties comparing model and observations, and the large impact of a snow layer on your simulations then?
»> During the 24. of March The average Sea ice surface registered by the KT19.85 was 251.7+/-3.5K. As the sensitivity analysis indicate, the assumption on snow thickness being a constant fraction of the sea ice thickness is a major source of uncertainty.

P4 L1-3. Can you provide a little more detail on this as its such a substantial bias?How do you know it was purely additive? How was this tested?
»>According to the campaign report Hendricks et al.2014 the bias was determined and corrected by taking measurements over open water and performing so called wing wags to cross calibrate the two antennae feeds. Also the RFI filtration system based on frequency and time sampling masked out the samples that were showing characteristics of an artificial source.

P4 L10. Here I found myself asking if you used the same roughness data from nadir to simulate the 45-degree return. This was answered much later but you should state it here.
»> corrected

P5 L2-3. How was the sea level estimated from lead tie-points? Do you have uncertainties for the sea level, freeboard and ice thickness, that you can apply to estimate uncertainties in modelled Tb? How did you estimate snow depth uncertainty when applying a simple snow scheme?
»> According to the campaign report Hendricks et al.2014, the tie points were picked manually giving the reference for the elevation measurements. The sea ice thickness is calculated from re-sampled to 1second ALS data, we took the standard deviation of the 1s sample as uncertainty. We estimate the snow thickness as a constant fraction of the sea ice thickness, thus we assume a propagation of uncertainty derived from elevation uncertainty.

L4. Do you use an iterative procedure to estimate ice thickness then, if the thickness is already required to estimate snow depth?
»> Unfortunately not, we assume a hydrostatic equilibrium and that the snow thickness is 1/10 of the ice thickness.

L11. Do you have a citation for the version of MILLAS used here, or was this added work completed as part of your study? If the latter, you need to describe model addi-tions including equations for review (perhaps in an appendix).
»> corrected. We included a short description in the manuscript.

L16. How are the ice and water salinities calculated? (You need to make it clear here that you use the ice surface T from airborne observations to constrain ice thermody-namics in the simulations). I'd like to see a table here of the constants used for ice,water and snow physical parameters, and then the range over which other

parameters(e.g. roughness) varied. »>Thank you for this suggestion, we include the formulas and constants used in MILLAS in the Table 1

L30-31. It's important here that you state ALS observations of roughness are averaged over quite a long window. As it's currently written, it sounds like you are simulating and comparing with measured returns over the exacts same 70 m window.

L34. Use a proper citation style for this reference.
»> corrected

P6 L4-5. Did you filter out all 70-m sections containing mixed classes, e.g. some open water? What about thin leads within the footprint? I'd expect many of your eventual 5-km sections contained at least some open water, so how was this accounted for?
»> We compute the surface roughness statistics from 70m section treating it as a one class. We exclude from the analysis the 1s sections with more than 5% missing data. This rather crude method assumes that thin ice or open water will not reflect the laser scanner resulting in missing data. An alternative would be to use the camera images, but those were not taken continuously.

L13. 'coast' »> corrected

P7 L1-2. I'd like to see a figure which proves this. This cutoff limit between anisotropic and isotropic orientation of surface features has not been shown before, so a novel result of this study. But if you want to prove there is a scale separation at 4.3 km you need to show the data
»> New section: Section 2.2.1 no describes the azimuth orientation of the facets along the flight track with the figure

L10. Can you show the exponential function fit to each class of data in Fig 3, so we can see how well it performs? Eq 9. What is R?
»> R is the distance from facet to the antenna, explanation is now added together with the fits. Although, we show three example of smooth; medium and rough ice as placing all the classes cluttered the figure.

In the latest version of the manuscript (submitted on 2019/10/31) we add the exponetial fits to the PDFs for the selected classes. (see figure 4). In the figures bellow we present the fits for all roughness classes.

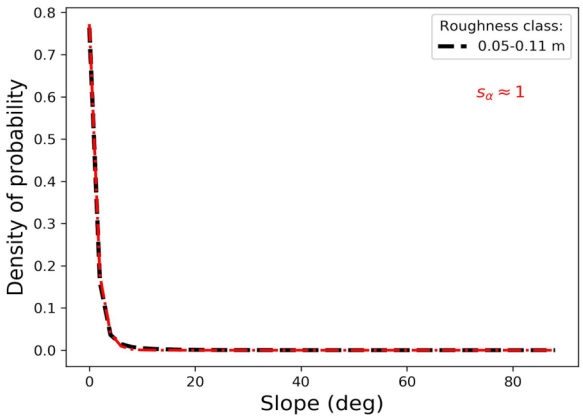
Roughness class:
0.05-0.11 m
$s_\alpha \approx 1$
Density of probability
Slope (deg)

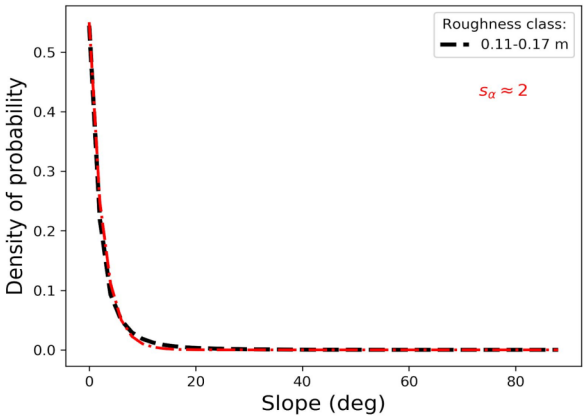
Roughness class:
0.11-0.17 m
$s_\alpha \approx 2$
Density of probability
Slope (deg)

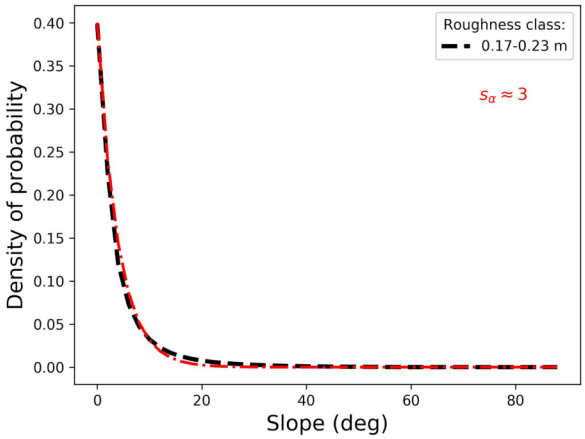
Roughness class:
0.17-0.23 m
$s_\alpha \approx 3$
Density of probability
Slope (deg)

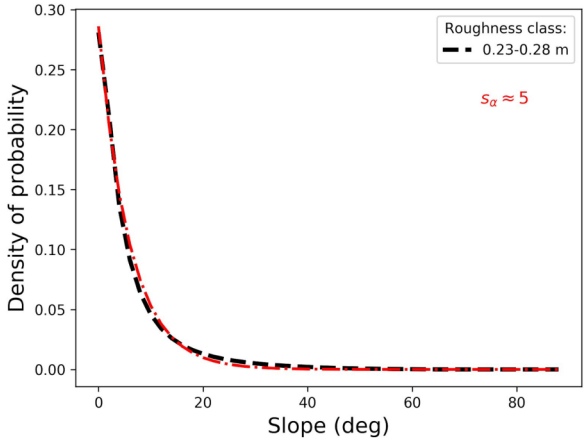
Roughness class:
0.23-0.28 m
$s_\alpha \approx 5$
Density of probability
Slope (deg)

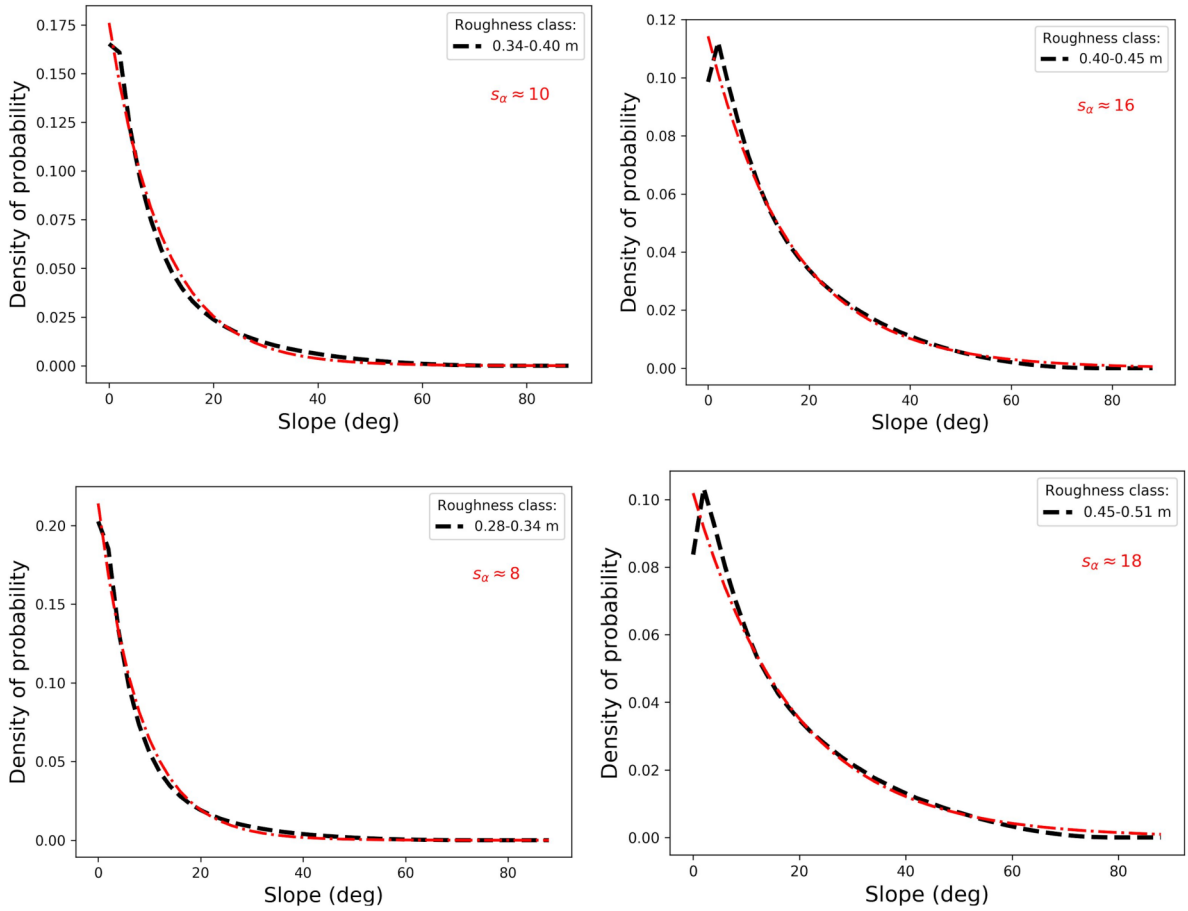

P10 L3-4. Is it reasonable to assume a constant gain pattern over the entire FOV? Do you have an estimate of the antenna pattern to compare to?
»> We do not have the antenna pattern for the setup during the campaign. It is possible to make assumptions about it based on the horn size, however when mounted on the plane the sidelobes and gain will vary. When considering the case of isotropic slope orientation the antenna gain can be considered constant.

L10. So the T profile is calculated directly from surface T and the reference constant salinity?
»> Yes, according to the formulas presented in Table 1: (after Untersteiner, 1964) Snow thermal conductivity = 0.31W/(mK) Ice thermal conductivity = 2.034 W/(mK)+0.13W/m * Sice(g/kg)/Tice(K) Ice salinity = 4 g/kg P12 L5. If you refer to angles in degrees within the text, the x-axis in Fig 6 should also be in degrees

L9. 'And'? »> corrected

L12-13. Confusing. What do you mean by this?

P13 L3. 'High'? »> corrected

P13 L16-31. I can't understand why this section is included, along with Figures 7 and 8.Why not just calculate reasonable variations in MILLAS emissivity for different sea icescenaios? E.g. warm/cold ice, different salinities, shallow/deep snow, different snowT or densities? Relative permittivities up to 10-20 are unrealistic for sea ice in most conditions, so they are not helpful for your analysis here. There's only really reason to show the cases listed directly on Line 24.

»> corrected, The section is reedited.

P15 L5. State this earlier in the method.

L7. How do you decide when it is needed?
»> corrected, refrazed

L8-9. Is the roughness CDF calculated from all altimeter observations within this 5-km window then?
»> yes. The CDFs are computed from all altimeter observations within 1s section that have less than 5% missing data.

P18 L8. Unlikely permittivity but possibly thickness. What about open water within footprints? Could that have affected the radiometer measurements? Or maybe snow depth/property variations along track?
»> The missing data criterion from previous point partially solves the problem of smooth thin ice or open water within the footprint. However, the sensitivity to open water is much greater than that to the surface roughness. Corrected to "...heterogeneous in terms of its thickness"

L9-10. You at least had the facet orientation info at least for the nadir looking antenna right? »> yes

Response to Reviewer 2

Regarding your remarks to the manuscript.

The discussion of Fig. 6 and its use for interpretation of the experiments is incomplete:One of the interesting results of Fig. 6 is that between 40and 45deg inc angle, the h-pol TBs are practically insensitive to the roughness parameter s. This is important for L band satellite sensors observing only at such incidence angles like SMAP (in orbit since 2015) and the upcoming CIMR, and for the airborne observations at 45deg(Figs. 9 and 10, Table 1): In the case when no influence of the roughness on the TB signal is expected (h-pol), the found correlation between observation and model is clearly higher, the RMSE, bias and the ubRMSE all are higher than at v-pol, where the model predicts a sensitivity to roughness. In Figs. 9(c) and 10(c), the h-pol 45inc angle cases, the modeled TBs show clearly less variability than the corresponding v-pol cases (Figs. 9(d) and 10(d)). Do you have an interpretation for this finding?

»>The comparison between the simulated and measured TB especially for the slide-looking antenna is not conclusive. First of all, we do not have the roughness information from the slide-looking footprint. We assume that the statistical distribution of facet geometries are the same as for the nadir one. Secondly, the assumption of the constant antenna gain over field of view is not adequate. The Geometrical roughness model describes the sub-footprint characteristics of the sea ice surface. Unfortunately, we do not have the measurements of the antenna gain functions when mounted on the aircraft. Thirdly, as indicated by the sensitivity the simulated TB is much more sensitive to the snow cover than to the surface roughness. However, due to the lack of independent snow measurements we resort to making assumptions about its thickness.

Fig. 6 and P12 L9-10 '..the horizontal and vertical polarization curves are brought together.' Correct only at incidence angles > 45. At lower angles, the opposite is the case. Best, add to Fig. 6 the polarization difference curves near the bottom, potentially at an increased y scale.

»>The polarization difference is now added as a subplot the Figure 7. (new figure numbering)

Fig.6: Give x axis in degree, not in rd because in text you use deg.

»>All angles are now given in degrees.

The current version of eq. (3) contains a product instead of a sum ('+' missing), and eq. (5) is incorrectly copied from Ulaby and Long, (2014), p443: replace $\hat{r}$ in nominator and in denominator by n, and check order of factors. r in this equation does not make sense at all: y should be independent of $\hat{r}$!

»>Thank you for double checking the equation 3 (eq. 4 in the current version of the manuscript). It is a typo, the antenna looking direction $\hat{r}$ is looking downwards, therefore a "-" in the z axis is added.

Equation 5 after Ulaby and Long 2014 p443 , in the book the n_i denotes the "direction of propagation" , which in our case is the "antenna look direction" $\hat{r}$. Probably my change of the notation contributed to confusion. In the manuscript the subscript "i" is reserved for the facet coordinates: n_i - facet normal, y_i and x_i coordinates on the facet's plane.

Units should be given in a consistent way throughout the whole manuscript. Here, the units m, cm and mm all occur, which is confusing and makes reading cumbersome. Have always a blank between number and units.
»>Units: all the distance units are now converted to meters and all units are formatted with the siunitx package, (eg. 273K)

The references in the text are frequently odd: if part of a sentence, then it should read'as found by Smith (1964)', and if not, it should read like '...was formerly shown (Smith,1964)'. Might be incorrect use of LaTeX commands cite and citep. References with two authors are cited like (Ulaby and Long 2014), not like (Ulaby et al.2014).
»>Citation formatting was corrected with more consistent use of "citep" and "citet" commands.

Abstract and main text should be in present tense, not past tense.Overall, I suggest accepting the paper after major revisions
»> The paragraphs are re-written in present tense.

Other points:

Page 2 L(ines) 12-15:roughness explanation too short to be understandable without further reading. Some questions: 'high pass filtering (cut off at 0.25m)': high pass filtering occurs in frequency domain, but you give a length as cut off.
»> With reference to the spatial frequency in L7 i changed the frequency unit to m^1

Give Fraunhofer criterion explicitly to make manuscript understandable without further reference.
»>The Fraunhofer criterion is now explicitly stated

P5L11 the current version of MILLAS takes into account multiple reflections: if this is new, then describe it in more detail.
»>An explanation about multiple reflections in MILLAS is added.

Fig. 2: indicate which columns are used for the three curves in Fig 3, e.g. by using the same colors as in Fig. 3. Fig. 3: give average values of slope, and give slope in deg instead of rad.Fig 4: indicate the values used for the three curves in Fig 3, e.g. by corresponding colors.
»>The color coding is introduced on figure 2, and subsequent.

P9L1: which is the direction of Phi_0: North? Flight direction?
»> the coordinates system is defined such as $\Phi_0 = 0$, ie. so as $\hat{x}$ is parallel to the ground and on the plane including the nadir and side looking antenna directions.

P9L5: "local" coordinate system is an unhappy name, as all coordinate systems introduced are centered at the footprint center. Suggestion: we introduce a tilted coordinate system with the same origin, but the z-coordinate aligned .. with $\hat{n_i}$.
»> As suggested, we reformulated. Now we use 'tilted' instead of "local".

Eq. (9): define A, R.
»>Eq9 Explanation added, A - facet area, R - distance 'antenna-facet'

Fig. 5: T_B H/V reads like a ratio, better call it e.g. T_B H,V. Explain ITS, CDF_alpha
»>Fig 5 Notation changed $T_B H,V$ instead of H/V, explanation of ITS and CDF is now added to the title.

Regarding "Minor points":

P(age) 1, L(ine) 11: take out incorrect blanks: 'on surface permittivity, second...'
»>P1L11 blanks taken out

P2L9: The incident wavelength reacts differently with individual components of the superimposed roughness: 1. Do you mean The incident radiation ? 2. Term superimposed roughness unclear. Do you mean roughness at different scales?
»> Rephrased, now: . . . "The incident radiation of a given wavelength reacts differently with individual components of the superimposed roughness of many scales..."

P3L30: 30% RFI contamination: in time or in signal energy?
»> 30% RFI contamination refers to the number of samples, this is now added to text.

P4L9: vertical, horizontal or both?
»> This is unclear to me, as it refers to the Airborne Laser scanner description.

P4L16: define ALS

»> the ALS abbreviation is now explained

P5L23 boned -> beyond,
»>Now corrected

P5L33 Reference: do not give first names, check bibtex file
»>Checked, and corrected

P8L9 “global” coordinate system in Cartesian basis (..)Cartesian coordinate system with the origin in the center of the sensor footprint
»>Changes as suggested

P12 end of L9: endand
»> corrected

P13L3: heighthigh
»> corrected

P13L23: Figures 7,8,Figures 7 and 8
»> corrected

P15L3: We want to determine the simulation setup that best reproduces....
»> corrected

P16L8: I do not find 4.5 K in Table 1. Do you mean 4.6 K?
»> Yes, corrected

P17L9: decreesdecreases
»> corrected

P17L10: decreaseddecreases, increasedincreases
»> corrected

P17L13: ..strongest for the roughest surface
»> corrected

P18L5: hadhas
»> corrected

P18L7: inclusion of a crude snow...; A possible explanation. . .
»> corrected

P18L11: the microphysical snow and sea ice properties
»> corrected

P18L13: on request
»> corrected

Marked-up manuscript

Effects of decimetre-scale surface roughness on L-band Brightness Temperature of Sea Ice

Maciej Miernecki[2,1], Lars Kaleschke[3,1], Nina Maaß[1], Stefan Hendricks[3], and Sten Schmidl Søbjærg[4]

[1]Institute of Oceanography (IfM), University of Hamburg, Bundesstr. 53, 20146 Hamburg Germany

[2]Centre d'Etudes Spatiales de la Biosphère (CESBIO), 18 avenue Edouard Belin bpi 2801, 31401 Toulouse Cedex 9, France

[3]Alfred Wegener Institute, Helmholtz Centre for Polar and Marine Research, Bremerhaven, Bussestrasse 24, 27570 Bremerhaven, Germany

[4]Technical University of Denmark, Ørsteds Plads, 2800 Kgs. Lyngby Danmark

Correspondence: Maciej Miernecki (maciej.miernecki@cesbio.cnes.fr)

Abstract.

Sea ice thickness ~~measurements with L-band radiometry allow for daily, weather-independent monitoring of the polar sea ice cover. The sea-ice thickness retrieval algorithms rely on the sensitivity of the L-band brightness temperature to sea-ice thickness. In this work, we investigate the decimetre-scale surface roughness as a factor influencing~~ is an Essential Climate Variable. Current L-Band sea ice thickness retrieval methods do not account for sea ice surface roughness that is hypothesized to be not relevant to the process. This study attempts to validate this hypothesis that has not been tested yet. To test this hypothesis, we created a physical model of sea ice roughness based on geometrical optics and merged it into the L-band ~~emissions from sea ice . We use an airborne laser scanner to construct a digital elevation model of the~~ emissivity model of sea ice that is similar to the one used in the operational sea ice thickness retrieval algorithm. The facet description of sea ice surface used in geometrical optics is derived from 2-D surface elevation measurements. Subsequently the new model was tested with T_B measurements performed during the SMOSice2014 field campaign. Our simulation results corroborate the hypothesis that sea ice surface ~~. We find~~ roughness has marginal impact on near-nadir T_B (used in the current operational retrieval). We demonstrate that the probability ~~density~~ distribution function of surface slopes ~~is exponential for a range of degrees of roughness. Then we apply the geometrical optics, bound with the MIcrowave L-band LAyered Sea ice emission model in the Monte Carlo simulation to simulate the effects of surface roughness. According to these simulations, the vertical polarization~~

around Brewster's angle is most affected by decimetre-scale surface roughness with brightness temperaturedecreasing up to 8 K . The horizontal polarization for the same configuration exhibits a 4 K increase. The near-nadir angles are little affected, up to 2.6 K decrease for the most deformed ice. These result indicate that the current operational sea ice thickness retrieval algorithm using the near-nadir can be approximated with a parametric function whose single parameter can be used to characterize the degree of roughness. Facet azimuth orientation is isotropic at scales greater than 4.3 km. The simulation results indicate that surface roughness is a minor factor in modeling the sea ice brightness temperature. The change in T_B is most pronounced at incidence angles greater than 40 degrees, and can reach up to 8 K for vertical polarization at 60 degrees. Therefore current and future L-band is marginally affected by omission of the surface roughness. Overall the effects of large-scale surface roughness can be expressed as a superposition of two factors: the change in intensity and the polarization mixing. The first factor depends on surface permittivity, the second shows little dependence on it. The sensitivity analysis indicates that snow cover impacts the brightness temperature to a greater extent than surface roughnessmissions (SMOS, SMAP, CIMR, SMOS-HR) measuring at such angles can be affected. Comparison of the brightness temperature simulations with the SMOSice2014 radiometer data does not yield definite results.

1 Introduction

The L-band brightness temperature (T_B) is sensitive to sea ice thickness. This feature is used for sea ice thickness retrieval from L-band T_B (over thin ice, <1.5 m) (Tian-Kunze et al., 2014; Huntemann et al., 2014; Kaleschke et al., 2016). Several factors influence T_B measurements over ice-covered regions, among them: ice concentration, ice temperature, snow cover, sea ice surface roughness and the shape of the interfaces between the snow and ice layers (Maaß et al., 2013; Ulaby, F. T. and Long, D. G. et al., 2014) (Maaß et al., 2013; Ulaby, F. T. and Long, D. G. et al., 2014, p. 422).

Here, we investigate the effects of surface roughness on the L-band T_B, specifically the large scale roughness. So far this factor is not included in the modeling of sea ice emissions in operational sea ice thickness retrieval. Electromagnetic scattering theory assumes that the roughness of a random surface is characterized by statistical parameters including standard deviation of surface height (σ_z), and correlation function ($R(\xi)$) measured in units of wavelength (Ulaby, F. T. and Long, D. G. et al., 2014) (Ulaby, F. T. and Long, D. G. et al., 2014, p. 422). These roughness statistical parameters are derived from measurements of surface elevation (z), conducted with altimeters that are characterized by their accuracy (δ) and sampling distance (Δx). As usual, the measurement method has an impact on the outcome, in this case by filtering out both high and low spatial frequencies of the surface roughness. Sea ice elevation measurements obtained from airborne altimeters (Ketchum, 1971; Dierking, 1995) and supplemented with terrestrial laser scanners (Landy et al., 2015) draw a picture of sea ice roughness as a multi-scale feature covering several orders of magnitude from large floes and pressure ridges (from tens to hundreds meters) to frost flowers and small ripples (in the centimeter to millimeter scale). The incident radiation of a given wavelength (λ) reacts dif-

ferently with individual components of the superimposed roughness of many scales ~~(Ulaby, F. T. and Long, D. G. et al., 2014)~~ (Ulaby, F. T. and Long, D. G. et al., 2014, p. 252).

At small end of the roughness spectrum i.e. when the change of surface elevation over sampling distance ($\Delta z/\Delta x$) is much smaller than λ ($\Delta z/\Delta x << \lambda$), the surface roughness is negligible. It means that the angular characteristics of scattered radiation are the same as for the secular surface. As a rule of thumb, Δx should be smaller than 0.1λ (Dierking, 2000). Sea ice roughness measurements with terrestrial lidar carried out by Landy et al. (2015) show that standard deviation of surface height σ_z ranges from $0.001\,\mathrm{m}$ to $0.0064\,\mathrm{m}$, after high-pass filtering (cut off at $4\,\mathrm{m}^{-1}$, Δx = $0.002\,\mathrm{m}$). These results indicate that, according to the Fraunhofer's smoothness criterion (σ_z<λ/32cosθ, where θ is the angle of incidence), most sea ice types (except artificially grown frost flowers) can be treated as a smooth surface for L-band at scales lower than $0.25\,\mathrm{m}$.

In this study, we focus on the other side of the roughness spectrum i.e. the large-scale surface roughness of sea ice ($\Delta z/\Delta x >> \lambda$). In this case, changes in surface elevation are not negligible and ~~their~~ alter the local incidence angle (θ_i). Studies of surface scattering by Lawrence et al. (2011, 2013) conclude that region of $8\lambda \times 8\lambda$ is sufficient to model small-scale roughness. Here, we assume that at larger spatial scales (larger then $8\lambda \times 8\lambda$) the surface roughness can be characterized in terms of geometrical optics (GO); for sea ice with $\epsilon_{ice} = 4.1$, $\lambda_{ice} = \lambda/\sqrt{\epsilon_{ice}} \approx 0.1\,\mathrm{m}$.

GO approximation describes the surface as a set of facets ~~(Ulaby, F. T. and Long, D. G. et al., 2014)~~(Ulaby, F. T. and Long, D. G. et al., 2 . This approach was applied for modeling the effective emissivities of mountainous terrain (Matzler and Standley, 2000) and ocean surface (Prigent and Abba, 1990). The latter study involved probability distribution of slopes in crosswind and downwind directions. A similar method was used in the context of sea ice to assess the uncertainties caused by roughness in sea ice concentration products derived from passive microwaves (Stroeve et al., 2006). Liu et al. (2014) measured ice surface slopes and other roughness statistics in the Bohai Sea. Their result was obtained with linear (1-D) scans under the assumption of isotropic roughness characteristics. The study by Beckers et al. (2015) has demonstrated that the statistics of sea ice roughness (mean z, σ_z, kurtosis and skewness) obtained from 1-D altimeter and 2-D laser scanner converge, on the condition that the surface is not strongly heterogeneous. Nonetheless, the 1-D altimeter data cannot properly represent the spatial orientation of surface facets. The surface facet orientation is characterized by both the slope (α) and the azimuthal angle in which it is facing (γ).

In this paper, we address the knowledge gap regarding the influence of large-scale surface roughness on L-band T_B. The paper comprises four main sections. The introduction, presenting the context is in Section 1.

Section 2 introduces the experimental data collected during SMOSice2014 campaign (section 2.1). Among them are the ~~airbore laser scanner elevation measurements for surface roughness characterization and~~ EMIRAD2 L-band radiometer T_B measurements, which will serve as reference for the T_B simulations. Another instrument is the airborne laser scanner (ALS) used for surface elevation measurements. The surface elevation measurements are used to construct a digital elevation model (DEM) of sea ice surface. From the DEM we derive the facet surface slopes and their orientation. In section 2.2 we analyze the statistics of the facet orientation. Based on facet orientation statistics, we derive a parametrization of the probability distribution function of surface slopes (PDF_α), that will serve as surface roughness representation in T_B simulations.

Section 2.3 presents the setup used for sea ice T_B simulation. For the simulation of the sea ice T_B we use the MIcrowave L-band LAyered Sea ice emission model (MILLAS) (Maaß et al., 2013). In section 2.4 we show how we integrate the surface roughness statistics (PDF_α) with MILLAS using geometrical optics.

The three key results of this study, namely (a)~~the T_B simulations for sea ice with different degrees of surface roughness~~ surface roughness reduces the polarization difference, this change is most pronounced at incidence angles greater than 50°, (b)~~the sensitivity study of the model~~ nadir T_B is little affected and (c)~~comparison of the EMIRAD-2 radiometer measurements with modeled~~ comparison with the radiometer data and sensitivity study indicate that snow cover has greater impact on the T_B ~~with and without roughness parametrization~~ than surface roughness are subsequently presented and discussed ~~(~~in section 3~~)~~.

Section 4 summarizes the results and discusses the implications of this study for current and future L-band missions.

2 Materials and Methods

In this section we present the SMOSice2014 campaign that is the key dataset of this study (subsection 2.1). Section 2.2 presents the sea ice surface roughness measurements in the context of geometrical optics. Section 2.3 presents the sea ice emission model that we used.

2.1 SMOSice2014 Campaign

The SMOSice2014 campaign took place between March 21, 2014 and March 27, 2014 in the area between Edgeøya and Kong Karls Land, east of Svalbard. Hendricks et al. (2014) and Kaleschke et al. (2016) described the campaign extensively. In this study we analyzed the data acquired during the flights on March 24/26. From this point ~~, onwards~~onwards, we focus solely on the parts relevant to the presented work.

In the period preceding the experiment from late January until early March the meteorological conditions in the region deviated strongly from the climatological means. The air temperature measured at Hopen Island meteorological station was on average 9 to 12°C higher than the climatological value for the period 1961-1990 (Strübing and Schwarz, 2014). Prevailing southerly winds pushed sea ice against the coasts of Nordaustlandet and into Hinlopen Strait, leaving a small strip of compacted ice along the coasts of Edgeøya. When sea ice returned with southerly drift in early March, the scene was set for the experiment. The thickest, most deformed ice was located in the western part of the studied region with a gradual decrease in thickness eastwards, where thin newly-formed ice was dominant. This pattern can be observed in the SMOS sea ice thickness product displayed in Figure 1a. In this work, we focus on the data from the low altitude flight at 70 m, because it is the data with highest spatial resolution of the Airborne Laser Scanner (ALS) among all the flights. The analysis was further reduced to the 24th of March, it is due to the fact that the region covered on the 26th of March had a discontinuous ice cover and a large scale swell was interfering with the surface elevation measurements. On March 24, the Polar 5 research aircraft of the Alfred Wegener Institute (Bremerhaven, Germany), undertook measurement flights starting from the eastern coast of Edgeøya, along the lines marked in red and green on Figure 1b. The figure also shows TerraSAR wide swath scenes, taken in the region. Flight A made between 10:05 and 10:41 UTC, flight B occured from 11:25 to 12:07 UTC. The set of instruments mounted

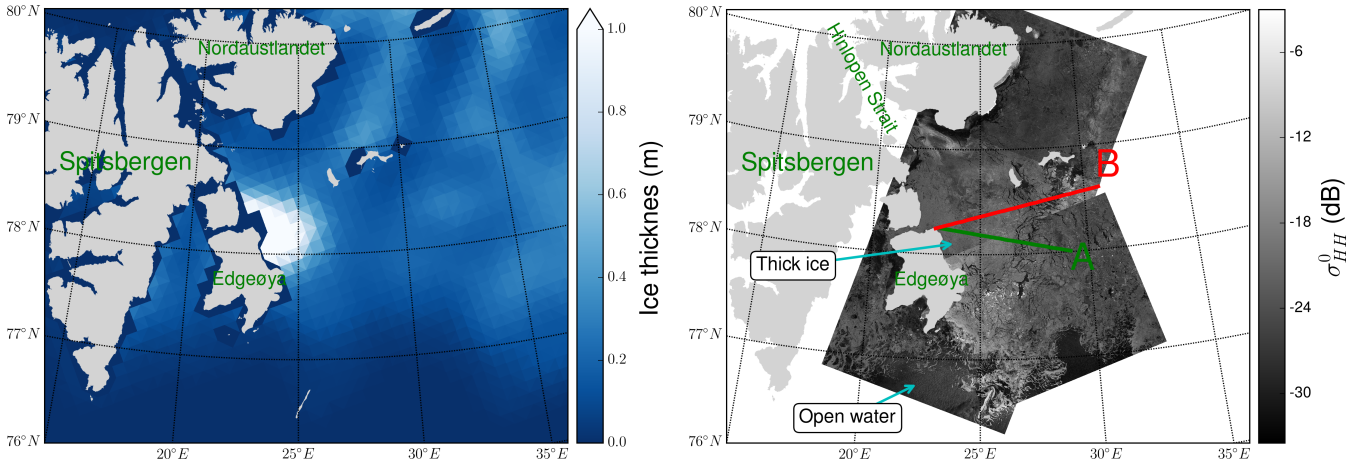

(a) Sea ice thickness on March 24 2014, derived from SMOS. The SMOS sea ice thickness product with a resolution of 40 km is presented on a 15 km grid. An aggregation of thick ice (>1 m) is visible along the Edgeoya's eastern coast.

(b) Sea ice conditions in the flight region on March 24. The TerraSAR-X wide swath mode (HH polarization), with frames taken at 05:35 UTC and 14:58 UTC. The aircraft tracks are marked in green - A at 10:05-10:41 UTC and red - B at 11:25-12:07 UTC.

Figure 1. The region of SMOSice2014 Campaign.

on the aircraft included an aerial camera to visually register the ice conditions, the Heitronics KT19.85 pyrometer for surface temperature measurements, the L-band radiometer EMIRAD-2, and the Airborne Laser Scanner (ALS) for high-resolution surface elevation measurements.

2.1.1 EMIRAD-2 Radiometer

The EMIRAD-2 L-band radiometer (developed by DTUSpace) is a fully polarimetric system with advanced radio frequency interference (RFI) detection features (Søbjaerg et al., 2013). The setup mounted on the aircraft consists of two Potter horn antennae, one nadir pointing, one side looking at 45°incidence angle. As the aircraft flew at the altitude of 70 m, the footprint of each antenna was 60 m × 90 m for the nadir pointing antenna, and 70 m × 90 m for the side looking antenna. The receiver's sensitivity is 0.1 K for a 1 s integration window. Along with the L-band measurements, navigation data was collected as to transform the polarimetric brightness temperature into the Earth reference frame (Hendricks et al., 2014). The EMIRAD-2 data was screened by evaluating kurtosis, polarimetric (Balling et al., 2012), and brightness temperature (T_B) anomalies. The screening showed RFI contamination for up to 30% of the samples. After subtracting of the mean value of the RFI-flagged data from the mean value of the full data, we found a 10 K difference for the nadir-looking horn, while the difference was non significant for the side looking horn. The analysis of the T_B during the "wing wags" calibration maneuvers further revealed a 20 K offset relative to the nadir-looking vertical channel caused by a continuous wave signal from the camera that was mounted on the airplane to obtain visual images. The analysis concludes a purely additive characteristic that allowed for bias correction (Hendricks et al., 2014). In this study, we use the data pre-processed by the DTU-team. The radiometer data was RFI cleaned and bias-corrected and validated using aircraft wing wags and nose wags over open ocean (Hendricks et al., 2014).

2.1.2 Airborne Laser Scanner

In this study, the ALS (Riegel VQ-580 laser scanner) has two purposes: (1) to measure the surface elevation for subsequent estimation of the ice thickness and (2) to characterize the surface topography. The ALS near-infrared laser (wavelength $1064\,\mathrm{nm}$) ~~is measuring~~ measures snow and ice elevation with the accuracy and precision of $0.0025\,\mathrm{m}$. Across-track and along-track elevation measurements were obtained every $0.25\,\mathrm{m}$ and $0.50\,\mathrm{m}$, respectively. These sampling characteristics resulted from the combination of the flight altitude ($70\,\mathrm{m}$) and the setup of the ALS (pulse repetition rate of $50\,\mathrm{kHz}$, cross track range of ± 30 degrees). The field of view of the radiometer side-looking antenna was only partially covered by the ALS scans. Nonetheless, we assume that the roughness characteristics measured by ALS are representative for both antennae ~~field of views~~fields of view. The data were calibrated and geo-referenced to the WGS84 datum. Further processing involved manual classification of tie points in leads in order to obtain local sea level and sea ice free-board (Hendricks et al., 2014). The geo-referenced surface elevations are used to compute surface roughness statistics. The elevation data is interpolated to a regular $0.5\,\mathrm{m}$ by $0.5\,\mathrm{m}$ grid to form a digital elevation model (DEM) of the sea ice surface. The DEM serves to derive surface slopes orientation.

The ~~typical set of~~ estimate of sea ice thickness was built on the hydro-static equilibrium assumption. The data required to estimate sea ice thickness consists of (a) the densities of water and ice, and (b) the snow load classically described by snow density and snow thickness, (c) ALS's free-board data.

The water, ice, and snow densities retained are $1027\,\mathrm{kg/m^3}$ (water) and $917\,\mathrm{kg/m^3}$ after Ricker et al. (2014), and $300\,\mathrm{kg/m^3}$ after Warren et al. (1999).

Snow thickness was meant to be provided by the onboard snow radar, however the equipment was still in test phase at the time of the experiment. As a workaround, we followed Kaleschke et al. (2016) and used the approximations found in Yu and Rothrock (1996) and Mäkynen et al. (2013)) that set the snow thickness to 10% of the sea ice thickness.

~~The actual estimate of sea ice thickness was built on the hydro-static equilibrium assumption, the above data, and the ALS's free-board data.~~

2.2 Sea Ice Surface Roughness

In this subsection we will analyze the data from the airborne laser scanner (ALS) that we presented in section 2.1.2. We use the ALS data to measure the ~~decimetre-scale~~ decimeter-scale surface roughness. The ALS is a laser instrument that measures the distance to the surface. ~~That surface is most likely to by snow laying on the ice . The~~ If snow covers the ice the ALS will register the snow-air interface as the elevation. Therefore, the relief of the ice is ~~therefore~~ modified by snow cover. During the SMOSice2014 campaign the snow measurements were unavailable. We assume that snow cover is a plane-parallel layer over sea ice. This assumption ~~do not accounts~~ does not account for snow dunes and drifts that may form on the ice. The implications of snow thickness on the radioactive transfer modeling are discussed in the section presenting the sensitivity analysis (section 3.2).

In the context of radiation transfer, the surface roughness is characterized in relation to incident wavelength. The ALS along-track spatial sampling of $0.5\,\mathrm{m}$ is a few times larger than the L-band wavelength in sea ice ($\lambda_{ice} = \lambda/\sqrt{\epsilon_{ice}} \approx 0.1\,\mathrm{m}$),

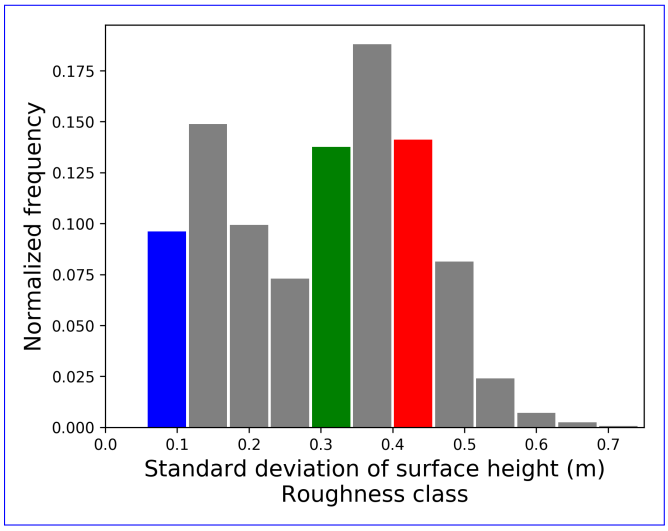

Figure 2. Histogram of the standard deviation of surface heights computed from 70 m flight strips, bins define the roughness classes of sea ice. Examples for three roughness classes "smooth", "medium rough" and "rough" are marked in colors blue, green and red, respectively.

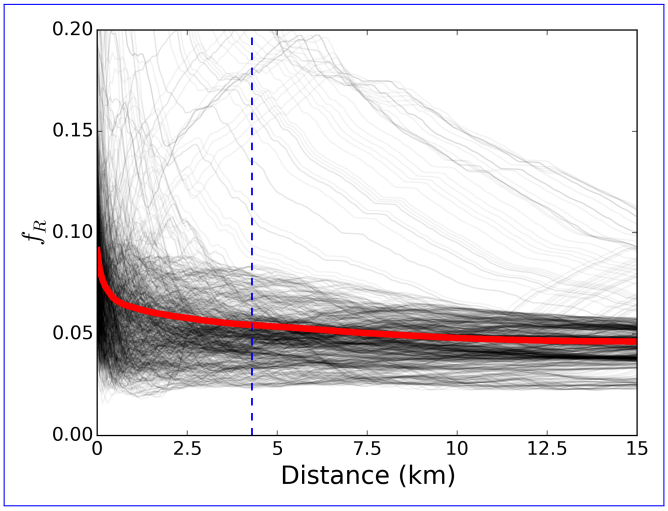

Figure 3. The f_R parameter illustrating the deviation from the uniform azimuth distribution along 1000 randomly selected samples. The average value of f_R is marked as thick red line. The considered threshold of uniform distribution 4.3 km is marked by blue dashed line.

which makes it suitable to measure the large-scale roughness, the part of the roughness spectrum where GO can be used to approximate the path of radiation. The analysis of ALS elevation data is done in three steps.

In the first step, we identify the ice with different degree of surface roughness. For that ~~,~~ purpose we divide the flight tracks into one-second sections (approximately 70 m long), large enough to cover the entire nadir radiometer footprint ~~,~~ and we build a histogram of the standard deviations of surface heights computed for these sections. The number of bins in the histogram is set according to the formula: $N_{bins} = 5\log_{10}(N_{data})$, after Panofsky and Brier (1958). We ~~decided on~~ chose standard deviation as ~~the~~ a criterion for defining the roughness classes, as it is widely used to characterize surface roughness from elevation profiles. Also, unlike visual interpretation of the aerial photography of sea ice it does not introduce personal biases. The resulting histogram in Figure 2 shows the sea ice roughness classes as histograms bins. No ~~strips~~ sections within the lowest standard deviation of surface height were found~~, that~~ . That is probably due to the fact that no refrozen lead of the scale of 70 m was found or the ALS laser signal was not reflected back from the surface resulting in missing data.

In the second step, we interpolate the ALS elevation measurements to a regular 0.5 m grid in order to form a digital elevation model (DEM) of the sea ice surface. The sea ice surface in the DEM is represented as a set of triangular facets. Each facet orientation in the 3D Cartesian space (for simplicity we assume the base vectors $\hat{x}, \hat{y}, \hat{z}$ to be aligned with the aircraft principal

axis, so $\hat{y}$ points to the flight direction), is described by two angles: facet slope α ($0 \leq \alpha < \pi$) and facet azimuthal direction γ ($-\pi \leq \gamma < \pi$). Therefore, the *i*-th facet local normal vector is described by:

$$\hat{n}_i = -\hat{x}\sin(\alpha_i)\cos(\gamma_i) - \hat{y}\sin(\gamma_i)\sin(\alpha_i) + \hat{z}\cos(\alpha_i) \tag{1}$$

In the third step, we compute the normal vectors and their orientations for the individual facets. This is done for all roughness classes. We found that the azimuthal orientation angle γ does not show any preferred directions within any given roughness class. ~~However, local elongated structures such as pressure ridges along the coast might have dominant directions of the slopes.~~ In the next subsections we present the analysis of the two angles characterizing the facet: azimuthal direction and surface slope.

2.2.1 Facet azimuth orientation

In the previous section we used the DEM to calculate the vectors normal to the surface facets. In this subsection we analyse the orientations of facet azimuths. In order to evaluate the distribution of the facet azimuths, we define parameter f_R (eq. 2). This parameter is calculated from a histogram of azimuth orientation. In eq. 2 the denominator is the total number of ~~samples under consideration~~ measurments expressed as the number of angular bins multiplied by the mean number of samples per bin (aka. total number of samples). The numerator is a sum of the differences between the mean number of samples per bin and the actual number of samples in each bin. There are 36 bins. The number of bins was determined with $N_{bins} = 5\log_{10}(N_{data})$ considering the maximal number of samples in $25\,\mathrm{km}$ flight track.

The f_R parameter equals to zero for the perfectly uniform distribution, in which case the number of counts in each bin (n_i) equals to a mean number of counts (μ). The f_R parameter reaches its maximum value of $f_{Rmax} = 2 - 4/N_{bins}$ when the slopes are aligned, i.e. grouped in two bins.

$$f_R = \frac{\sum_i^{N_{bins}}(|n_i - \mu|)}{N_{bins}\mu}, \qquad \mu = \frac{1}{N_{bins}}\sum_i^{N_{bins}} n_i \tag{2}$$

To evaluate f_R we selected 1000 random $15\,\mathrm{km}$ samples from the flight tracks. The analysis of the samples shows that the deviation from the uniform distribution decreases sharply with increasing distance over first kilometer (figure 3). For ~~distance along the sample~~ distances along the flight track greater than 4.3 km the curve flattens at value of $f_R = 0.05$ in 90% of the samples. We assume that at scales greater than 4.3 km(marked by vertical dashed line on figure 3) slope orientations do not have a preferential direction beyond natural variability. This distance corresponds to approximately $60\,\mathrm{s}$ ~~sections~~section. In figure 3 the average value of f_R is marked as thick red line. Several sample profiles are plotted in gray lines to illustrate the variability.

~~The f_R parameter illustrating the deviation from the uniform azimuth distribution along 1000 randomly selected samples. The average value of f_R is marked as thick red line. The 4.3 km threshold of uniform distribution is marked by blue dashed line.~~

2.2.2 Facet slope angle

Section 2.2.1 looked at the ~~the~~ azimuthal orientation of surface facets. This section focuses on the analysis of facet slopes. For all roughness classes we observe a similar probability density function (PDF) of surface slopes. The PDFs have a maximum at zero and a gradual decline in the likelihood of encountering the steeper slopes. Figure 4 shows the PDF_α in a logarithmic scale for the three distinct roughness classes: smooth $0.05\,\mathrm{m} < \sigma_z < 0.11\,\mathrm{m}$ (in blue), medium rough $0.28\,\mathrm{m} < \sigma_z < 0.34\,\mathrm{m}$ (in green) and rough $0.45\,\mathrm{m} < \sigma_z < 0.51\,\mathrm{m}$ (in red).

~~Density of probability of surface slopes in logarithmic scale for three roughness classes: smooth $0.05\,\mathrm{m} < \sigma_z < 0.11\,\mathrm{m}$ (in blue), medium rough $0.28\,\mathrm{m} < \sigma_z < 0.34\,\mathrm{m}$ (in green) and rough $0.45\,\mathrm{m} < \sigma_z < 0.51\,\mathrm{m}$ (in red). The exponential fits to the respective curves are marked in thin color dotted lines.~~

We decide to approximate the PDF of surface slopes with an exponential curve:

$$PDF_\alpha = C_{norm} \exp(-(\alpha / s_\alpha)), \tag{3}$$

where C_{norm} is the normalization constant and s_α is the "geometrical-slope roughness parameter". Figure 4 presents the data and the exponential approximations. The log scale is very relevant because it becomes obvious that the chances of encountering steep slopes are getting slimmer the higher the slope angle. Consequently, it makes sense that the approximation functions misfit the observations at high slope angles as it is irrelevant to fit an approximation there. As s_α is the only parameter of the approximation function, it is descriptive of the surface roughness.

Figure 5 shows the relation between s_α and the standard deviation of surface heights corresponding to the roughness classes defined above. The error bars represent the uncertainty associated with each data point. Very rough ice has large uncertainty ~~,~~ because the number of samples was small (classes with $\sigma_z > 0.6\,\mathrm{m}$, accounted for less than $75\,\mathrm{s}$ of flight, out of total $78\,\mathrm{min}$). The quadratic relation is holding well for ice with up to $0.5\,\mathrm{m}$ standard deviation of surface heights. The equation of the fitted curve is: $s_\alpha = 51.61\sigma_z^2 + 1.50\sigma_z + 0.14$

2.3 Sea Ice Brightness Temperature Simulation

In this subsection we present the emission model for simulating the sea ice brightness temperature (T_B). We use the MIcrowave L-band LAyered Sea ice emission model described by Maaß et al. (2013), further referred to as MILLAS. This model is based on the radiative transfer model of Burke et al. (1979) (who used it for soils), with infinite half-space of seawater covered with layers of sea ice, snow and a top semi-infinite layer of air. In contrast to the original model of Burke et al. (1979) and its usage by Maaß et al. (2013), the current version of MILLAS takes into account multiple reflections at the layer boundaries. The

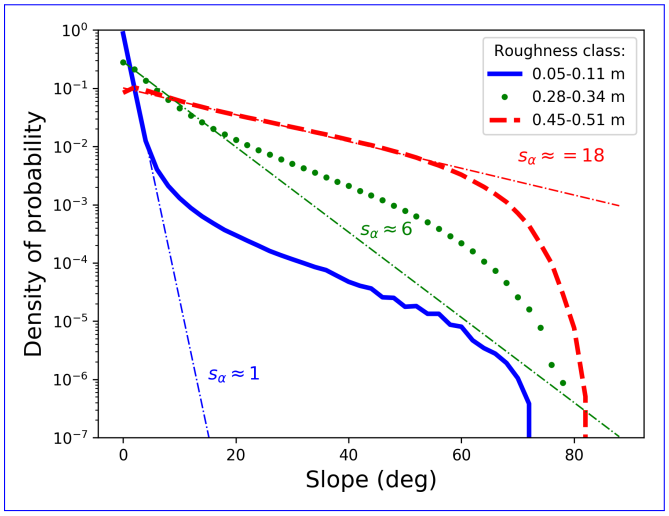

Figure 4. Density of probability of surface slopes in logarithmic scale for three roughness classes: smooth $0.05\,\mathrm{m} < \sigma_z < 0.11\,\mathrm{m}$ (in blue), medium rough $0.28\,\mathrm{m} < \sigma_z < 0.34\,\mathrm{m}$ (in green) and rough $0.45\,\mathrm{m} < \sigma_z < 0.51\,\mathrm{m}$ (in red). The exponential fits to the respective curves are marked in thin color dotted lines.

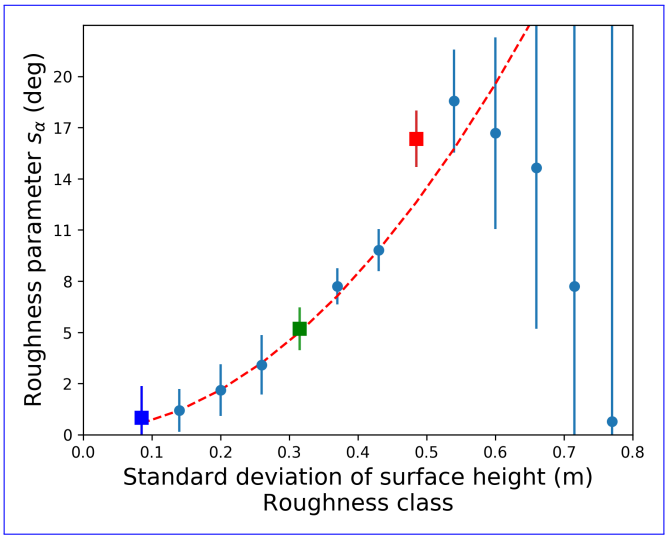

Figure 5. Surface roughness parameter s_α describing the probability distribution of surface slopes. Error bars are inversely proportional to the number of data points in each roughness class. The "smooth", "medium rough" and "rough" classes are marked in colors blue, green and red, respectively. The red dashed line marks the fitted curve.

multiple reflections are expressed as subsequent terms of a geometric series. The summation over series stops when terms of the series contribute less than a given threshold to the total (in following calculations the threshold was set to 0.001). MILLAS describes the brightness temperature above snow-covered sea ice as a function of temperature and permittivity of the layers. The water permittivity depends mainly on the water temperature and salinity (Klein and Swift, 1977). Ice permittivity can be approximately described as a function of brine volume fraction (Vant et al., 1978), which depends on ice salinity and the densities of the ice and brine (Cox and Weeks, 1982), which in turn depends mainly on ice temperature. We set the ice salinity to $4\,\mathrm{g/kg}$ which is a mean value for first year ice determined by Cox and Weeks (1974). The permittivity of dry snow can be estimated from its density and temperature (Tiuri et al., 1984). In the simulation, the ice and water salinity are kept constant (see Table 1)~~, furthermore~~. Furthermore, we assume that the system is in thermal equilibrium ~~,~~and that the water beneath the ice is at the freezing point. In this configuration, the T_B is simulated as a function of ice thickness (d_{ice}), snow thickness (d_{snow}) and surface temperature (T_{surf}). In our setup, the snow is assumed to be dry with a density of $300\,\mathrm{kg/m^3}$, that is the average snow density value for December Arctic measurements from 1954-91 Warren et al. (1999). The T_B simulations are only slightly sensitive to snow density, see Figure 3 in Maaß et al. (2013). The permittivities of snow and ice are linked to their temperature. The temperature profiles within snow and ice are assumed to be continuous and linear. The values for the ice and snow thermal conductivity are taken from Yu and Rothrock (1996); Untersteiner (1961). As the optimization of the emission model lies beyond the scope of this work, we use the simplest setup variant of MILLAS consisting of a single layer of ice covered with a single layer of snow.

Table 1. Brightness temperature simulation setup of the **MI**crowave **L**-band **LA**yered **S**ea ice emission model ($MILLAS$).

	Parameter	Value
Snow	surface temperature	**measured** (KT19)
	snow wetness	0%
	snow density	300 kg/m^3
	snow thermal conductivity	0.31 W/(mK)
Ice	ice thermal conductivity	2.034 W/(mK) + 0.13 W/m $\cdot$S$_{ice}$ (g/kg)/T_{ice}(K)
	ice salinity	4 g/kg
Water	water salinity	33 g/kg
	water temperature	271.2 K

2.4 Simulation of Brightness Temperature of Rough Sea Ice

In the previous sections, we described the sea ice surface as composed of facets with an orientation described by two angles: the slope α and the azimuthal direction γ. Subsequently, we analyzed the ALS data to extract information about statistical distributions of slopes and their orientation. We concluded that the exponential function is suitable to describe the probability density function of surface slopes for a range of ice surfaces with different degree of surface roughness.

In this section, we describe how we integrate the probability description of faceted sea ice surface with the MILLAS emission model. We will start by describing the coordinate system that we used in the T_B simulations. The relations between radiometer antenna-look direction ($\hat{r}$) and the horizontal ($\hat{h}$) and vertical ($\hat{v}$) polarization vectors are described in Cartesian coordinate system. We show how these ~~relation~~ relations are represented in the coordinate system associated with a facet. The vectors defined in the tilted facet coordinate system are denoted with the subscript *i*. Subsequently, we will derive the equation that sums up the emissions originating from multiple facets.

~~The~~ We consider the Cartesian coordinate system ($\hat{x}$, $\hat{y}$, $\hat{z}$) with the origin in the center of the nadir sensor footprint. In this reference frame the radiometer antenna-look direction ($\hat{r}$) is described as:

$$\hat{r} = \hat{x}\sin(\theta_0)\cos(\phi_0) + \hat{y}\sin(\theta_0)\sin(\phi_0) - \hat{z}\cos(\theta_0), \tag{4}$$

where the θ_0 is the antenna incidence angle and the ϕ_0 is the azimuthal direction of the antenna~~, in~~. In this particular case we set the reference system so as $\phi_0 = 0$ ~~,~~and $\hat{x}$ is parallel to the ground. The antenna setting defines the directions of the horizontal ($\hat{h}$) and vertical ($\hat{v}$) polarization vectors:

$$\hat{h} = -\hat{x}\sin(\phi_0) + \hat{y}\cos(\phi_0), \qquad \hat{v} = -\hat{x}\cos(\theta_0)\cos(\phi_0) - \hat{y}\cos(\theta_0)\sin(\phi_0) - \hat{z}\sin(\theta_0). \tag{5}$$

We are interested in finding a relationship between the radiation originating from a tilted ~~face of the facet and the~~ facet and from a flat one. For that ~~porpouse~~ purpose we must consider the tilted coordinate system associated with *i*-th facet (variables associated with individual facets are denoted with subscript *i*). The z-coordinate in this tilted coordinate system is aligned with the facet normal vector $\hat{n}_i$, followed by $\hat{x}_i$ and $\hat{y}_i$ calculated accordingly:

$$\hat{z}_i = \hat{n}_i \qquad \hat{y}_i = \frac{\hat{n}_i \times \hat{r}}{|\hat{n}_i \times \hat{r}|} \qquad \hat{x}_i = \hat{y}_i \times \hat{z}_i \tag{6}$$

Therefore, the local incidence angle θ_i is:

$$\theta_i = \cos^{-1}(-\hat{r} \cdot \hat{n}_i) \tag{7}$$

and the local horizontal and vertical polarization vectors are:

$$\hat{h}_i = \hat{y}_i, \qquad \hat{v}_i = -\hat{x}_i \cos(\theta_i) - \hat{z}_i \sin(\theta_i) \tag{8}$$

The emissions from the facet at an angle θ_i and polarization *p* are denoted with an asterisk: $T_B^*(\theta_i; p)$. In order to calculate the brightness temperatures observed in the global horizontal and vertical polarization it is necessary to account for the coordinates rotation ~~(Ulaby, F. T. and Long, D. G. et al., 2014)~~(Ulaby, F. T. and Long, D. G. et al., 2014, p. 443):

$$T_{Bi}(\theta_i; H) = (\widehat{h} \cdot \widehat{h}_i)^2 T_B^*(\theta_i; H) + (\widehat{h} \cdot \widehat{v}_i)^2 T_B^*(\theta_i; V) \tag{9a}$$

$$T_{Bi}(\theta_i; V) = (\widehat{v} \cdot \widehat{h}_i)^2 T_B^*(\theta_i; H) + (\widehat{v} \cdot \widehat{v}_i)^2 T_B^*(\theta_i; V) \tag{9b}$$

We model the sea ice surface as a set of facets~~, therefore~~. Therefore the brightness temperature registered at the antenna aperture is a sum of contributions from N facets. We assume that each facet area A, at the distance R is visible at the incidence angle θ_i and covers a patch of antenna field of view, equal to the solid angle Ω_i:

$$\Omega_i = \frac{A \cos(\theta_i)}{R^2 \cos(\alpha_i)} \tag{10}$$

The formula summing the contributions from N visible facets is:

$$T_B(\theta_0;p) = \frac{1}{N\cos(\theta_0)} \sum_{i=1}^{N} \omega_i T_{Bi}(\theta_i;p)\Omega_i \tag{11}$$

with ω_i the antenna gain component.

At this stage of our study, we aim at modeling the effect of surface roughness on the T_B. As a first order approximation we assume that ~~that~~ the antenna gain is constant across the whole field of view and that the antenna is in a far field so the incidence angle θ_0 is assumed constant across the field of view. This assumption is more suitable for the space-born system. The resulting formula is:

$$T_B(\theta_0;p) = \frac{1}{N\cos(\theta_0)} \sum_{i=1}^{N} T_{Bi}(\theta_i;p)\sec(\alpha_i)(-\hat{r}\cdot\hat{n}_i) \tag{12}$$

This is the formula that we implement in the geometrical roughness model. Figure 6 presents the data flow in the geometrical roughness model. The model merges the ~~the~~ MILLAS emission model (suitable for sea ice) with the geometrical characterization of the faceted surface. In the presented setup the MILLAS emission model uses the sea ice surface temperature ($T_{surface}$), sea ice thickness (d_{ice}) and snow thickness (d_{snow}) as input variables. The GO part needs the cumulative probability distribution of surface slopes (CDF_α) and the antenna look direction ($\hat{r}$). The orientation of N facets representing the sea ice surface is calculated with the inverse transform sampling (ITS) (Devroye, 2006). This method returns a random slope value from a given non-uniform distribution. The non-uniform distribution is described by a cumulative probability distribution, which in this case depends on the geometrical roughness parameter s_α. Similarly, the azimuthal angle γ_i is drawn from a uniform distribution. The result of this processing step is the set of N pairs of angles (α_i, γ_i) describing the orientation of N facets. In the next step, the local normal vector and the local incidence angle (θ_i) are calculated for each of the N facets. The θ_i is used ~~for calculating~~ to calulate the brightness temperature emitted from the *i*-th facet with the emission model. Shadowing occurs when $\theta_i > \pi/2$ and the radiation is emitted away from the antenna. In the current setup the double-bounce effects are not accounted for. $\hat{r}$ and $\hat{n}_i$ are used to calculate the local and global polarization directions, as well as Ω_i. For the final step, the summed contributions from N facets are summed as in the equation 12. The result is the brightness temperature of the surface observed under θ_0 and polarization p.

The number of facets N impacts ~~on~~ the quality of the simulation and the reproducibleity of the results. In order to set the value of N we looked at the standard deviation of 20 T_B simulations results for nadir and 45 degrees. We decided that the standard deviation of T_B should be lower than 0.1 K, as this is the accuracy of the EMIRAD-2 radiometer for the one second integration time. This criterion is met for N greater than 10^4, which we take as the N value for further simulations.

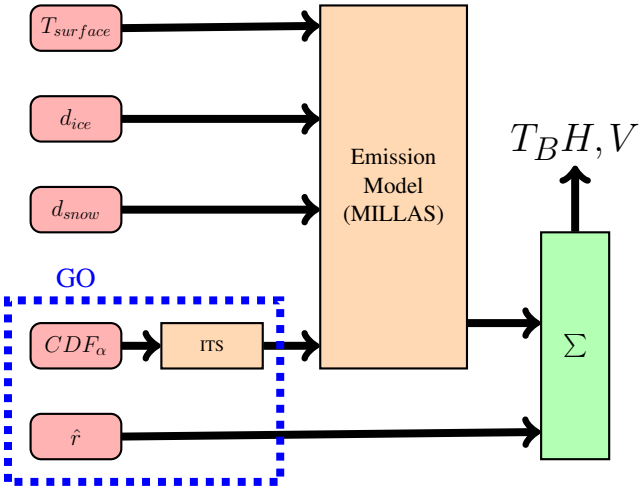

Figure 6. Flowchart showing the processing chain within the geometrical roughness model. The model consists of two principal blocks: the emission model ~~,~~ and the inverse transport sampling ITS module responsible for generating the facet orientation. ~~Input~~ The input parameters: surface temperature $T_{surface}$, ice thickness d_{ice}, snow thickness d_{snow}, cumulative distribution of surface slopes CDF_α, antenna direction $\hat{r}$ are colour coded in red.

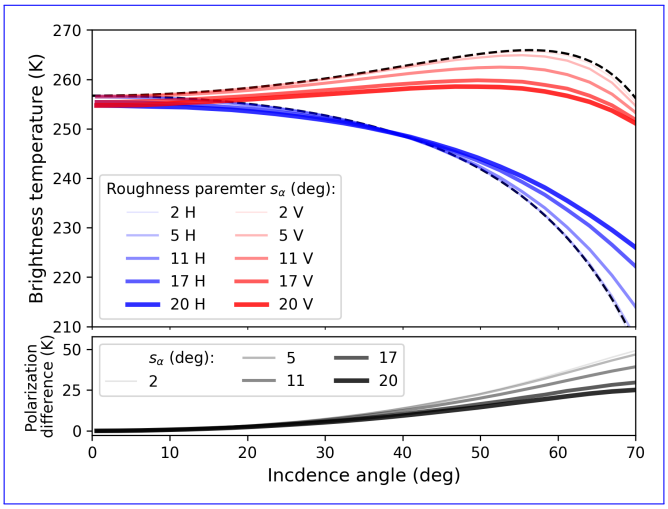

Figure 7. Effects of the large-scale surface roughness on the brightness temperature of sea ice, simulated with geometrical roughness model. Vertical polarization in red, horizontal in blue. The black dashed lines mark the T_B for the specular surface. The surface roughness parameter s_α varies between 2 to 20, the thicker the line the higher the s_α. The inputs for the MILLAS emissivity model are kept constant: $T_{surface}$=260 K, $dice$ =1.42 m, d_{snow} =0.14 m.

3 Results

The three main results of this study are: (~~1~~a) surface roughness ~~reduced~~ reduces the polarization difference, this change is most pronounced at incidence angle greater than 50°, (~~2~~b) nadir T_B is little affected and (~~3~~c) comparison with the radiometer data and sensitivity study indicate that snow ~~cower~~ cover has greater impact on the T_B than surface roughness.

In section 3.1 we show the brightness temperature simulations for sea ice with different ~~degree~~ degrees of large-scale surface roughness. To interpret the results we make a sensitivity analysis (section 3.2). The comparison of the simulated vs. measured T_B over 4.3 km flight track samples is shown in section 3.3.

3.1 Brightness temperature simulations

In section 2.2.2 we derived a parametrization of the degree of surface roughness. We approximate the roughness by an exponential probability distribution function (PDF) of surface slopes. The shape of the PDF is fully described by the s_α parameter.

In our simulation s_α varies between 2 and 20 ~~,~~ in accordance with the measurements of surface slopes done during the SMOSice2014. As the aim of this study is to characterize the effect of surface roughness on L-band T_B, in this section we keep the other parameters ~~in~~ of the emissivity model constant: surface temperature and ice and snow thickness ~~constant~~ ($T_{surface}$ =260 K, d_{ice} =1.42 m, d_{snow} =0.14 m). The brightness temperatures are calculated for every degree of incidence angle in range 0-70 degrees. Figure 7 shows the simulation results.

~~Effects of the large-scale surface roughness on the brightness temperature of sea ice, simulated with geometrical roughness model. Vertical polarization in red, horizontal in blue. The black dashed lines mark the T_B for the specular surface. The surface roughness parameter s_α varies between 2 to 20, the thicker the line the higher the s_α. The inputs for the MILLAS emissivity model are kept constant: $T_{surface}$=260 K, $dice$ =1.42 m, d_{snow} =0.14 m.~~

The effect of increasing surface roughness is two-fold. First, the overall near-nadir intensity is lowered by 2.6 K. Second, the polarization difference decreases. For the highest value of the roughness parameter, at Brewster's angle the vertical polarization decreases by 8 K ~~,~~ and horizontal polarization experiences a 4 K increase. The effect of roughness is more pronounced for larger values of roughness parameter s_α and is most visible at higher incidence angles (60°).

The polarization mixing can be explained by the approach used in this study. The emissions from the facet in horizontal ($\widehat{h}_i$) and vertical ($\widehat{v}_i$) polarizations are partially mixed when expressed in the $(\widehat{h}, \widehat{v})$ coordinate system (see eq. 12).

The lowering of the intensity has two possible explanations. First is that our model ~~do~~ does not take into account shadowing effects. When local incidence angle is greater than 90°, the facet is emitting away from the antenna. For the "near-nadir" angles (~~0-30°~~)0°-30°), the likelihood of shadowing is less than 1% for the most rough ice (see fig. 4).

~~Second~~ The second explanation of this effect is associated with shape of the Fresnel emissivity curves. The polarization difference for large incidence angles is larger than for the near-nadir ones. Therefore, the mean of the two polarizations $(T_B(\theta_0; H) + T_B(\theta_0; V))/2$ i.e. total intensity) is fairly constant up to 30°and than drops ~~sharply by~~ continuously $\sim$ 10 K by 60°. The trend continues for higher incidence angles. High values of s_α increase the likelihood of returning a large incidence angle in the inverse transform sampling. These large incidence angles contribute to the overall lowering of the T_B. The contribution of this mechanism is $\approx$2 K for $T_B(0)$ in case of the most rough ice. The 2 K estimate was obtained by integrating the drop in total intensity weighted by the PDF_α.

The above results are obtained with a Monte Carlo simulation. This method is a time consuming approach. Therefore, we propose a parametrization of the simulation results. The two effects: the polarization mixing and the lowering of brightness temperature ~~,~~ can be expressed in a fashion similar to the HQ model proposed by Choudhury et al. (1979). Here we propose a formulation with two parameters H_α and Q_α.

$$T_B(\theta; p) = [(1 - Q_\alpha) \cdot T_B^*(\theta; p) + Q_\alpha T_B^*(\theta; q)] \cdot H_\alpha \tag{13}$$

where p and q stand for the polarization.

H_α accounts for the change in total intensity and Q_α for the polarization mixing. The emissions from the specular surface are denoted with an asterisk: ~~$T_B^*(\theta; p/q)$~~$T_B^*(\theta; p, q)$. The proposed parametrization approximates the results obtained with the Monte Carlo simulation with a root mean square difference of 0.45 K

$$H_\alpha = a_1 s_\alpha^2 + a_0 \qquad Q_\alpha = b_1 s_\alpha^2 + b_0 \tag{14}$$

where $a_1 = 0.018 \times 10^{-3}$, $a_0 = 1$ and $b_1 = 0.532 \times 10^{-3}$, $b_0 = 0$.

The emissions from the specular surface are an essential input for the geometrical roughness model used in this study. The exact shape of the simulated brightness temperature curves depends on the probability distribution of slopes ~~,~~as well as on the emission characteristics of the specular surface. In this paragraph, we will investigate how the shape of the ~~$T_B^*(\theta;p/q)$~~ $T_B^*(\theta;p,q)$ influences the geometrical roughness model results. The shapes of the polarization curves i.e. the reflectivities for a given incidence angle, are described by the Fresnel equations. Equations that are determined by the permittivity of the medium (ϵ). (In this ~~work~~ section we omit the question of penetration depth assuming that the emissions are coming from the isothermal ice layer of constant permittivity). To investigate the impact of the varying ϵ we take a range of permittivities specific to sea ice ~~,~~as calculated within the MILLAS model. In the present setup the sea ice ~~permitivity~~ permittivity depends on bulk ice salinity and ice temperature. We calculate the ϵ for a range of ice temperatures ($250\,\mathrm{K} < T_{ice} < 271\,\mathrm{K}$) and salinities ($1\,\mathrm{g/kg} < S_{ice} < 12\,\mathrm{g/kg}$).

The sea ice permitivities from the MILLAS model range between ϵ = 3.1 + 0.05i (for T_{ice} =271 K, S_{ice} =7 g/kg) and ϵ = 4.6 + 0.8i (for T_{ice} =253 K, S_{ice} =1 g/kg), where T_{ice} is the bulk ice temperature and S_{ice} is the bulk ice salinity. The curves corresponding to those values lie close together indicating that the proposed parametrization is suitable for all types of sea ice. The effect of permittivity on the polarization mixing parameter (Q_α) is less pronounced. The dependence of the Q_α parameter on the roughness follows a similar quadratic curve regardless of the surface permittivity.

3.2 Sensitivity analysis

In this section, we investigate ~~the sensitivity of our model . This step will enable the interpretation of the results of the comparison between simulations and measurements presented in section 3.3. We start by estimating the sensitivity to sea ice contrition. Than we progress to analyze the model inputs~~how sensitive the model is to its main variables: surface temperature, ice thickness, snow thickness, surface roughness and the implicit assumption of 100% sea ice concentration. This is a mandatory step toward the evaluation of the model (section 3.3).

The two most important factors influencing the L-band brightness temperature over sea ice are the ice concentration and the ice thickness. We calculate the sensitivity of our model with regard to sea ice concentration by assuming a linear mixing of water and thick ice fractions within the radiometer footprint. The brightness temperature of sea water T_{Bw} (salinity of 33 g/kg, temperature 271.2 K) is approximately 110 K and ~~$T_{Bi}(0,p/q)$~~ $T_{Bi}(0;p,q)$ of thick sea ice (T_{surf} =260 K, d_{ice} =1.5 m, bulk salinity of 3 g/kg) is 240 K. The resulting sensitivity to sea ice concentration is $\approx 1.5\,\mathrm{K}/\%$.

The sensitivity of the T_B to sea ice thickness over thin sea ice ($d_{ice} < 0.75$ m) is fundamental for the sea ice thickness retrieval from L-band radiometry. ~~It is only~~ T_{Bi} saturates when the sea ice thickness is significantly larger than the penetration depth of the L-band radiation~~when the T_{Bi} saturates~~. Therefore, our analysis focuses on sea ice thicker than 1 m, in order to single out the contributions of surface roughness~~, our analysis is concentrated on sea ice thicker than 1 m~~.

Table 2 contains the sensitivities of the geometrical roughness model to the input parameters: roughness parameter ~~s_{alpha}~~ s_α, ice thickness d_{ice}, snow thickness d_{snow} ~~,~~and surface temperature T_{surf}. Presented values are grouped into columns corresponding to the polarization and three incidence angles: 0°, 45°and 60°. The angles ~~where~~ are chosen to reflect the antennae

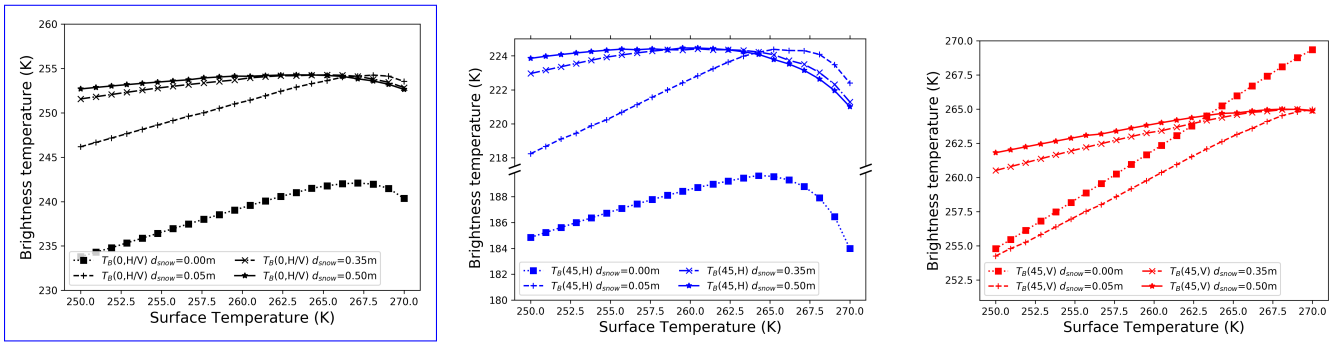

(a) Horizontal or vertical polarization at 0°: $T_B(0)$

(b) Horizontal polarization, incidence angle 45°: $T_B(45, H)$

(c) Vertical polarization, incidence angle 45°: $T_B(45, V)$

Figure 8. Change in the brightness temperature as predicted by the MILLAS emission model as a function of surface temperature. The different line styles ~~co respond~~ correspond to the different snow thickness assumptions. The calculation was done for the sea ice thickness of one meter and surface roughness set to zero.

configuration during the SMOSice2014 with an ~~additional~~ addition of 60°, close to Brewster's angle where surface roughness effects are most pronounced.

The assumption about snow thickness has a considerable effect on the sea ice T_B (Maaß et al., 2013). For this reason the values of sensitivities are considered for a number of snow thickness values. Figures 8a, ~~8~~ 8b and 8c show the simulated L-band brightness temperature at 0°, 45°as a function of the surface temperature. In ~~presented~~ this study we make considerable ~~assumption~~ assumptions about snow thickness. To illustrate the ~~assumptions the plots~~ uncertainty associated with the assumptions, the simulations are made for a range of snow thicknesses ~~in corresponding~~ plotted in different line styles.

In the MILLAS model, ice permittivity is parameterized with ice temperature. The non-monotonic shape of the curves is caused by change in ice permittivity. Therefore, ~~in table 2 the relevant values of sensitivities are given for~~ the sensitivities are calculated for two temperature ranges: lower (250 K-265 K) and higher (265 K-270 K)~~temperature ranges.~~

~~The assumption about snow thickness has a considerable effect on the sea ice T_B (Maaß et al., 2013). For this reason the values of sensitivitiesare considered for a number of snow thickness values~~. Table 2 contains the calculated sensitivities.

As far as the large-scale surface roughness is concerned, the sensitivity increases almost linearly for the values of s_α between 0°and 20°which is the maximal value measured during the SMOSice2014 campaign.

~~Change in the nadir brightness temperature as predicted by the MILLAS emission model as a function of surface temperature. The different line styles correspond to the different snow thickness assumptions. The calculation was done for sea ice thickness of one meter and surface roughness set to zero.~~

In order to interpret the results of the ~~simulation-measurements comparison~~ comparison between the simulation and measurements, it is necessary to evaluate the uncertainties associated with the input parameters: surface temperature, ice thickness and snow thickness. In the following paragraphs~~we by~~ , we use "mean model sensitivity for the cold conditions" ~~we understand~~ for the averaged absolute sensitivity ~~for~~ of $T_B(0; H, V)$ and $T_B(45; H, V)$ at 250 K. We take the values for the lower temperature ~~rage as they reflect~~ range as they match the conditions during SMOSice2014 campaign.

Table 2. Table with sensitivities of the brightness temperature at nadir, 45°and 60°as simulated with Geometrical Optics surface roughness model. The input parameters: roughness parameter s_{alpha}, ice thickness d_{ice}, snow thickness d_{snow}, surface temperature T_{surf}.

	$T_B(0;H,V)(K)$		$T_B(45;H)(K)$		$T_B(45;V)(K)$		$T_B(60;H)(K)$		$T_B(60;V)(K)$	
$\partial/\partial s_\alpha$ | d_{snow}=0	-0.01 to -0.20		0.06 to 0.80		-0.08 to -1.20		0.11 to 1.70		-0.14 to -2.10	
$\partial/\partial s_\alpha$ | d_{snow}=0.1m	-0.01 to -0.21		0.02 to 0.30		-0.05 to -0.74		0.05 to 0.77		-0.08 to -1.19	
$\partial/\partial s_\alpha$ | d_{snow}=0.25m	-0.01 to -0.21		0.02 to 0.33		-0.05 to -0.76		0.05 to 0.80		-0.14 to -1.22	
$\partial/\partial s_\alpha$ | d_{snow}=0.35m	-0.01 to -0.21		0.02 to 0.34		-0.05 to -0.77		0.05 to 0.82		-0.14 to -1.24	
$\partial/\partial s_\alpha$ | d_{snow}=0.45m	-0.01 to -0.21		0.02 to 0.35		-0.05 to -0.78		0.05 to 0.83		-0.14 to -1.25	
$\partial/\partial s_\alpha$ | d_{snow}=0.5m	-0.01 to -0.21		0.02 to 0.37		-0.05 to -0.79		0.05 to 0.85		-0.14 to -1.26	
range (K)	250-265	265-270	250-265	265-270	250-265	265-270	250-265	265-270	250-265	265-270
$\partial/\partial d_{ice}$	-0.91	2.05	0.18	3.49	-1.77	0.16	0.58	3.28	-2.12	-1.24
$\partial/\partial d_{snow}$	8.51	-2.03	6.58	-3.18	10.71	0.23	5.68	-2.45	10.10	0.89
$\partial/\partial T_{surf}$ | d_{snow}=0	0.50	-0.43	0.4	-0.95	0.61	0.15	0.29	-1.32	0.69	0.66
$\partial/\partial T_{surf}$ | d_{snow}=0.1m	0.34	-0.23	0.3	-0.5	0.41	0.02	0.26	-0.63	0.44	0.19
$\partial/\partial T_{surf}$ | d_{snow}=0.25m	0.18	-0.38	0.12	-0.59	0.24	-0.11	0.09	-0.68	0.27	0.05
$\partial/\partial T_{surf}$ | d_{snow}=0.35m	0.11	-0.39	0.05	-0.61	0.17	-0.16	0.01	-0.66	0.21	-0.01
$\partial/\partial T_{surf}$ | d_{snow}=0.45m	0.06	-0.40	0.01	-0.58	0.13	-0.19	-0.03	-0.67	0.17	-0.05
$\partial/\partial T_{surf}$ | d_{snow}=0.5m	0.05	-0.40	0.01	-0.57	0.11	-0.19	-0.05	-0.66	0.15	-0.06

The uncertainty associated with surface temperature is estimated as the product of the sensitivity of the model times the measurement uncertainty. The surface temperature measurements done with the KT19.85 have an accuracy of $0.5\,\mathrm{K}$. The mean surface temperature in the region covered by ice was $251.7 \pm 3.5\,\mathrm{K}$. We take the standard deviation of surface temperature measurements as the parameter uncertainty. ~~Then we multiplied the parameter uncertainty by average absolute model sensitivity at low temperatures to obtain the model uncertainty associated with it. Thus, we estimate the uncertainties~~ We estimate the uncertainty associated with surface temperature ~~is~~ to be $0.7\,\mathrm{K}$.

The uncertainty associated with sea ice thickness is estimated as the product of the sensitivity of the model times the measurement uncertainty. The sea ice thickness measurements in this study are derived from the re-sampled ALS elevation data. The mean standard deviation of the re-sampled elevation measurements is $0.08\,\mathrm{m}$. The assumption about the densities of snow, ice and water combined with the assumption on the snow thickness of 1/10 of ice thickness are leading to the

uncertainty of $0.4\,\mathrm{m}$. ~~Therefore, taking~~ Taking into account the mean model sensitivity for the cold conditions prevailing during the flights~~we estimate~~ , we estimate that the uncertainty associated with sea ice thickness is $0.5\,\mathrm{K}$.

The uncertainty associated with snow thickness is estimated as the product of the sensitivity of the model times the measurement uncertainty. Unfortunately, the snow thickness measurements are not available. The snow layer, although transparent for the L-band radiation, is not invisible. The refraction on the snow-ice and snow-air interfaces alters the local incidence angles. Snow cover also has an effect on the temperature profile within the ice. This indirectly affects the permittivity of sea ice. All these factors make an estimation of the uncertainty caused by snow thickness especially hard to quantify. We assume that snow thickness uncertainty is equal to the mean standard deviation of the re-sampled elevation measurements, that is $0.08\,\mathrm{m}$. The mean model sensitivity to snow thickness for the cold conditions is $8.6\,\mathrm{K/m}$. Therefore, we estimate the uncertainty associated with snow thickness to be $0.7\,\mathrm{K}$.

An important factor which is not directly included in the model is the sea ice concentration. In the model we assume ~~the~~ sea ice concentration to be 100% in order to single out the much smaller contribution of surface roughness. However, if a linear mixing model is applied the sensitivity to sea ice ~~contraction~~ concentration is $-1.5\,\mathrm{K/\%}$. During the ~~pre-procesing~~ pre-processing of the airborne laser scanner (ALS) data we excluded the ~~seventy meter~~ seventy-meter sections with more than 5% missing values. The missing values are caused by the instrument setup (rotating mirror, edge of swath) or by the lack of return reflection from open water or thin ice. We estimate that the uncertainty associated with the sea ice concentration is up to $7.5\,\mathrm{K}$.

To put the partial ~~sensitivity in to~~ sensitivities into perspective, the expected changes in the T_B caused by the strongest surface roughness ~~during~~ measured during SMOSice2014 ~~campign~~ campaign do not exceed $-2.2\,\mathrm{K}$ for nadir and $1\,\mathrm{K}$ and $-5.6\,\mathrm{K}$ for the horizontal and vertical polarization of the 45°antenna, respectively.

To conclude, the sensitivity analysis of the geometrical roughness model leads to the conclusion that ~~on the scale of one radiometer footprint (70 m)~~ the surface roughness effects will be hard to observe in the SMOSice2014 flights data with the current emission model setup.

3.3 Simulations vs. Measurements

In this section, we compare the brightness temperature measured with the EMIRAD-2 radiometer with the brightness temperature simulations. The comparison is done on a $4.3\,\mathrm{km}$ section as to justify the assumption of the isotropic azimuth distribution. We want to determine the simulation setup that best reproduces the radiometer measurements. And whether the inclusion of the surface roughness in the simulation brings significant improvement. The limitation of this approach is that we assume that the ice observed by the side looking antenna and the ice below the flight path have the same properties. We consider the surface temperature, the sea ice thickness and the surface roughness along the flight and we use them to run the statistical roughness model, described in section 2.4 with MILLAS single ice layer setup as the brightness temperature module. In setups including snow layer, the snow thickness is set to be 10% of the sea ice thickness. The calculation is done for $60\,\mathrm{s}$ averages, during which the aircraft covers the distance of approximately $4.3\,\mathrm{km}$. ~~For each~~ At this scale we consider the surface slopes orientation to be isotropic. The measured surface slopes are used to compute empirical CDF_α. Analysis at $4.3\,\mathrm{km}$ scale is justified by the fact

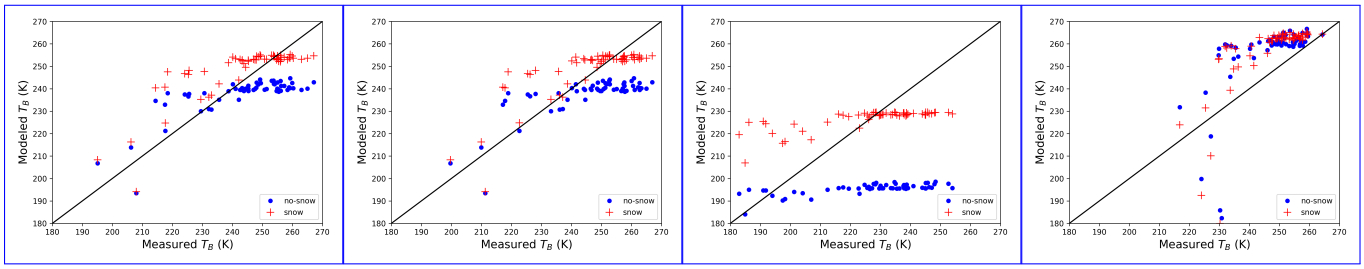

(a) $\theta = 0$, p=H (b) $\theta = 0$, p=V (c) $\theta = 45$, p=H (d) $\theta = 45$, p=V

Figure 9. ~~Scatter-plots~~ Scatter plots illustrating the comparisons between the EMIRAD-2 data and the T_B simulated without GO roughness included - **specular**. Results corresponding to the setup with snow are marked in green, without snow in blue.

that the antennae gains are not known. Furthermore, the averaged sea ice properties are more representative for the space-born radiometers.

For each radiometer channel we made four simulation setups~~,~~ : two without roughness ~~:~~(Flat no- snow, Flat snow), and two with roughness included: (Rough (GO) no-snow, Rough (GO) snow). As for the performance metrics of the model setups, we use the coefficient of determination (r^2), the root-mean-square error (RMSE) ~~, the bias and unbiased root- mean-square error (ubRMSE)~~and bias. These metrics are widely used in the assessment of the performance of satellite measurements (Entekhabi et al., 2010). Table 3 ~~holds~~ contains the results of the comparison expressed in terms of r^2, RMSE ~~, bias and ubRMSE~~and bias. The corresponding scatter-plots illustrating the comparison between measured and modeled brightness temperatures are presented on ~~the Figure ??~~figures 9 and 10.

The values of r^2 for all "channel - simulation setup" combinations do not exceed ~~0.3~~0.36. The simplified one-layer model managed to capture only ~~30~~36% of the signal variance even with surface roughness included. Furthermore, the inclusion of surface roughness brings little improvement to the statistics. In case of vertical polarization, where the model studies indicate the most sensitivity to roughness, the r^2 is even a little lower. The inclusion of a very crude snow thickness parametrization is more successful in capturing the radiometer measurements variability. All metrics show that the four model setups perform poorly in reproducing the EMIRAD-2 measurements. ~~The bias is the lowest for the side-looking vertical channel (up to 5 K). For the nadir channel the inclusion of snow in the model reduces the bias by 11 K to the value of 1.5 K. For the horizontal polarization channel the inclusion of snow has an opposite effect, changing the absolute value of bias from 4.6 K to −13.2 K. The high values of RMSE and ubRMSE show a general miss-fit of the model to the data.~~

The results of the comparison are also presented in the form of histograms of the difference between the measured and simulated T_B (figure 11). For all four antenna feeds the ~~difference~~ RMSE between simulated and measured T_B decreases whenever the setups include snow. However, the bias gets higher.

The high values of RMSE and bias show a general miss-fit of the model to the data. The sensitivity study of the model presented in section 3.2 indicates that the effects of surface roughness are of comparable magnitude or smaller than uncertainties associated with the model input parameters. The side looking vertical polarization is predicted to be most affected by the surface roughness. However, the surface roughness is not measured directly in side-looking antenna footprint. The scatter plots

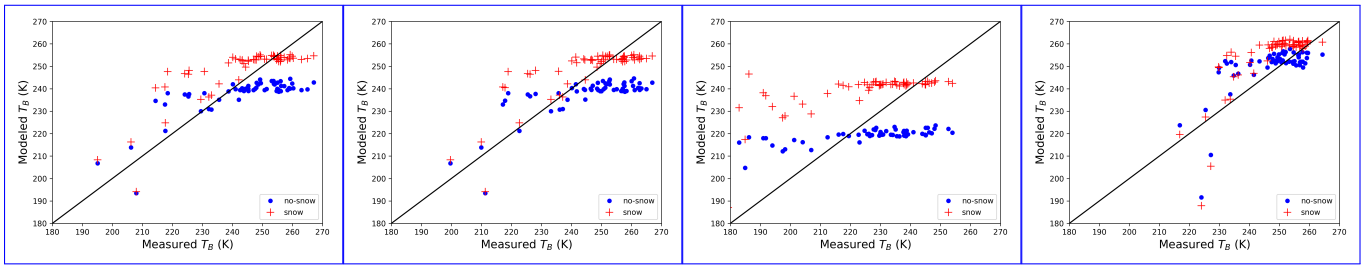

(a) $\theta = 0$, p=H (b) $\theta = 0$, p=V (c) $\theta = 45$, p=H (d) $\theta = 45$, p=V

Figure 10. ~~Scatter-plots~~ Scatter plots illustrating the comparisons between the EMIRAD-2 data and the T_B simulated **with GO roughness included**. Results corresponding to the setup with snow are marked in green, without snow in blue.

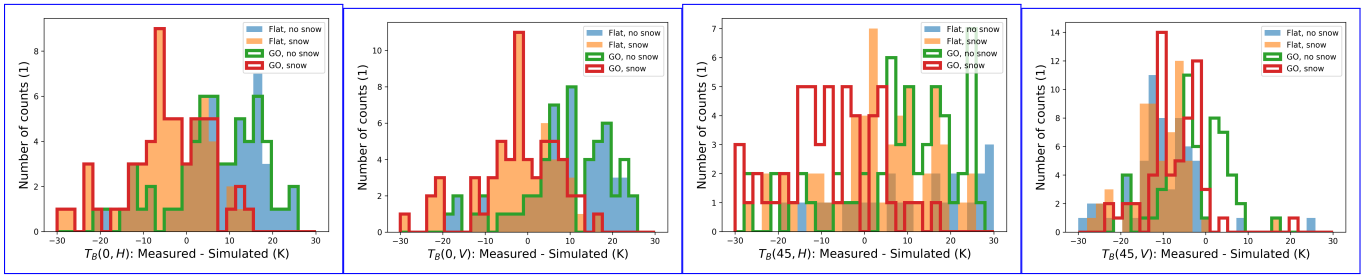

(a) $\theta = 0$, p=H (b) $\theta = 0$, p=V (c) $\theta = 45$, p=H (d) $\theta = 45$, p=V

Figure 11. Histograms of the differences between the EMIARAD2 measurements and simulation setups for four antenna feeds.

on figures 9 and 10 and the calculated statistics show that a simplified one-layer model struggles to capture the dynamics of the sea ice T_B regardless of the simulation setup.

4 Discussion and Conclusions

In this paper we address the knowledge gap concerning the influence of the ~~decimetre-scale~~ decimeter-scale surface roughness on the ~~L band~~ L-band brightness temperature of sea ice. We used the airborne laser scanner (ALS) data to characterize the sea ice surface and to produce the digital elevation model (DEM) of the sea ice surface. From the DEM we derived the probability distribution of surface slopes (α) and their azimuthal orientation (γ). We found that the probability distribution function of α (PDF_α) can be described with an exponential function regardless of the degree of roughness of sea ice surface. The exponent parameter (s_α) is a quasi-quadratic function of the standard deviation of surface heights. In the second part of this work, we used the PDF_α in ~~the~~ a Monte Carlo simulation of the emission from a faceted sea ice surface. The effect of surface roughness is ~~little noticeable in~~ marginal at near-nadir, accounting for up to 2.6 K decreases in T_B. The polarization curves around Brewster's angle are most affected. The vertical polarization decreases by 8 K and horizontal polarization increases by 4 K for the roughest ice, compared with the specular sea ice surface. The effect of the large-scale surface roughness on polarization curves is not linear with the degree of the surface roughness described by s_α. Meaning that the alteration of

Table 3. Performance ~~of~~ metrix for the different T_B simulation setups in terms of coefficient of determination r^2, RMSE (K), bias ~~K, ubRMSE~~ (K). For EMIRAD-2 channels four model setups are tested: Flat no snow, Flat snow, ~~Rough~~ GO no snow, ~~Rough~~ GO snow.~~Nadir-looking antenna channels are treated together.~~

Setup	$T_B(0,H)$			$T_B(0,V)$			$T_B(45,H)$			$T_B(45,V)$				
~~Flat, no snow~~	~~0.21~~ r^2	~~30.9~~ RMSE (K)	~~12.6~~ bias (K)	~~27.81.5ex~~ r^2	~~Flat, snow~~ RMSE (K)	~~0.29~~ bias (K)	~~26.1~~ r^2	~~1.3~~ RMSE (K)	~~26.7~~ bias (K)	~~Rough,~~ r^2	RMSE (K)			
Flat, no snow	~~0.20~~ 0.27	~~30.8~~ 27.2	~~12.5~~ 11.7	~~27.8 1.5ex~~0.26	~~Rough, snow~~ 28.5	~~0.29~~ 6.8	~~26.2~~ 0.22	~~1.5~~ 41.7	~~26.1~~ 71.3	0.19	26.7			
Flat, ~~no~~ snow	~~0.22 29.9 4.6~~ 0.36	~~29.5 1.5ex~~23.7	~~Flat, snow~~ -18.2	~~0.30~~ 0.35	~~30.3~~ 24.1	~~-13.2~~ 23.9	~~27.3 1.5ex~~0.33	~~Rough, no snow~~ 25.0	~~0.22~~ 68.5	~~29.8~~ 0.29	~~4.5~~ 25.2			
~~Rough, GO,~~ no snow	~~0.30 30.3 -13.2~~ 0.27	27.3	~~Flat, no snow~~ 12.3	~~0.16~~ 0.25	~~29.1~~ 28.5	~~4.0~~ 7.4	~~28.9 1.5ex~~0.26	~~Flat, snow~~ 28.2	~~0.24~~ 78.2	~~27.2~~ 0.19	~~-1.9~~ 26.0			
~~Rough, no~~ GO, snow	~~0.15~~ 0.36	~~29.3~~ 23.7	~~5.0~~ -17.8	~~28.9 1.5ex~~0.35	~~Rough, snow~~ 24.1	~~0.22~~ -23.4	~~27.1~~ 0.34	~~-1.2~~ 27.2	~~27.1~~ 72.2	0.28	24.7			

~~1.5ex~~

the T_B curves is strongest for the roughest surface. The overall change of emission due to the large-scale surface roughness can be expressed as a superposition of change in intensity (H_α) and an increase in polarization mixing (Q_α). The change in intensity depends primarily on the surface permittivity, whereas the polarization mixing shows little dependence on ϵ. ~~The paramtrization~~ This parametrization is suitable for all types of sea ice. However, the sensitivity analysis of the simplified emission model demonstrates that the expected change in T_B is comparable in magnitude to the uncertainty associated with the model input parameters.

The results have implication for the current and future L-band missions. The operational SMOS sea ice thickness product relies on near-nadir T_B observations (~~0-30°), therefore~~ 0°-30°). Therefore, the large scale surface roughness will have little effect on the retrieval. ~~Especially as the method is used with thin sea ice which tends to be smooth. While the~~ The SMAP and CIMR missions, ~~which~~ that operate at incidence angles of 40°and 55°, respectively, are more exposed to the surface roughness effects. ~~However, as the effect on~~ The effect on the vertical polarization is stronger than on ~~horizontal polarization, for SMAP $T_B(40,H)$ the influence is close to zero~~the horizontal polarization. Lastly, we compared the simulation of the brightness temperature (with and without surface roughness) with the radiometer measurements. Unfortunately, this showed that our model is not capturing the brightness temperature variability at the scale of 4.3 km~~flight track~~. The inclusion of surface

roughness is less important than the inclusion of a crude snow thickness parameterization. This is confirmed by the sensitivity analysis of the model. Another possible explanation is that the sea ice in the studied region was highly heterogeneous in terms of its thickness and snow cover. Furthermore, a simple two-layer emission model used in this study has its limitations in capturing the T_B variability. Better ~~result~~ results might be obtained if a multi-layer model together with the snow thickness measurements is used. With such setup the direct inclusion of sea ice facets orientation in the radiometer field of view will be a valuable option to improve the T_B simulation. ~~This however,~~ However, this would require in-situ measurements of sea ice permittivity, snow thickness, temperature and roughness as well as detailed characterization of the antenna gain. Thus, the authors recommendation for future studies is to measure the microphysical snow and sea ice properties together with surface roughness directly in the radiometer's field of view.

Code and data availability. Code and data are available from the authors on request.

Author contributions. Conceptualization, M.Miernecki and L.Kaleschke; Methodology, M.Miernecki; Software, M.Miernecki and N.N.Maaß; Validation, M.Miernecki, N.Maaß; Formal Analysis, M.Miernecki and L.Kaleschke; Investigation, M.Miernecki; Resources, L.Kaleschke; Data Curation, S.Hendricks, S.S.Søbjrg; Writing—Original Draft Preparation, M.Miernecki; Writing—Review & Editing, L.Kaleschke, N.Maaß ; Visualization, M.Miernecki; Supervision, L.Kaleschke; Project Administration, L.Kaleschke; Funding Acquisition, L.Kaleschke

This research was funded by the HGF Alliance, Remote Sensing and Earth System Dynamics. The European Space Agency co-financed the AWI research aircraft Polar 5 and helicopter flights (ESA contract 4000110477/14/NL/FF/lf; PI S.Hendricks) and the development and validation of SMOS sea ice thickness retrieval methods (ESA contracts 4000101476/10/NL/CT and 4000112022/14/I-AM; PI L.Kaleschke). Technical University of Denmark (DTU) co-financed and conducted the measurements with EMIRAD2 L-band radiometer on Polar 5.

Competing interests. The authors declare no conflict of interest. The founding sponsors had no role in the design of the study; in the collection, analyses, or interpretation of data; in the writing of the manuscript, and in the decision to publish the results

Acknowledgements. The authors acknowledge the institutions providing the data and people involved in carrying out the measurements. The TerraSAR-X and TanDEM-X teams provided the SAR data for this study.

Special thanks to Dr. Yann Karr, PI of the SMOS mission, for his suggestions and comments. As well as the financial support that covered the publication costs.

The following abbreviations are used in this manuscript:

ALS	Airborne Laser Scanner
CDF	Cumulative Distribution Function
DEM	Digital Elevation Model
GO	Geometrical Optics
ITS	Inverse Transform Sampling
MILLAS	MIcrowave L-band LAyered Sea ice emission model
PDF	Probability Distribution Function
RFI	Radio Frequency Interference
SAR	Synthetic Aperture Radar
SMAP	Soil Moisture Active and Passive Mission
SMOS	Soil Moisture and Ocean Salinity Mission
T_B	brightness temperature

References

Balling, J. E., Søbjaerg, S. S., Kristensen, S. S., and Skou, N.: RFI detected by kurtosis and polarimetry: Performance comparison based on airborne campaign data, in: 2012 12th Specialist Meeting on Microwave Radiometry and Remote Sensing of the Environment, MicroRad 2012 - Proceedings, 2012.

Beckers, J. F., Renner, A. H. H., Spreen, G., Gerland, S., and Haas, C.: Sea-ice surface roughness estimates from airborne laser scanner and laser altimeter observations in Fram Strait and north of Svalbard, Annals of Glaciology, 56, 235–244, https://doi.org/https://doi.org/10.3189/2015AoG69A717, 2015.

Burke, W. J., Schmugge, T., and Paris, J. F.: COMPARISON OF 2. 8- AND 21-cm MICROWAVE RADIOMETER OBSERVATIONS OVER SOILS WITH EMISSION MODEL CALCULATIONS., J Geophys Res, 84, 287–294, https://doi.org/10.1029/JC084iC01p00287, 1979.

Choudhury, B. J., Schmugge, T. J., Chang, A., and Newton, R. W.: EFFECT OF SURFACE ROUGHNESS ON THE MICROWAVE EMISSION FROM SOILS., Journal of Geophysical Research, 84, 5699–5706, https://doi.org/10.1029/JC084iC09p05699, 1979.

Cox, G. F. and Weeks, W. F.: Salinity variations in sea ice, Journal of Glaciology, 13, 109–120, 1974.

Cox, G. F. N. and Weeks, W. F.: EQUATIONS FOR DETERMINING THE GAS AND BRINE VOLUMES IN SEA ICE SAMPLES., CRREL Report (US Army Cold Regions Research and Engineering Laboratory), 1982.

Devroye, L.: Chapter 4 Nonuniform Random Variate Generation, in: Simulation, edited by Henderson, S. G. and Nelson, B. L., vol. 13 of *Handbooks in Operations Research and Management Science*, p. pp. 83–121, Elsevier, https://doi.org/10.1016/S0927-0507(06)13004-2, 2006.

Dierking, W.: Laser profiling of the ice surface topography during the Winter Weddel Gyre Study 1992, Journal of Geophysical Research, 100, 4807–4820, 1995.

Dierking, W.: RMS slope of exponentially correlated surface roughness for radar applications, IEEE Transactions on Geoscience and Remote Sensing, 38, 1451–1454, https://doi.org/10.1109/36.843040, 2000.

Entekhabi, D., Reichle, H. R., Koster, D. R., and Crow, T. W.: Performance metrics for soil moisture retrievals and application requirements, Journal of Hydrometeorology, 11, 832–840, https://doi.org/http://dx.doi.org/10.1175/2010JHM1223.1, 2010.

Hendricks, S., Steinhage, D., Helm, V., Birnbaum, G., Skou, N., Kristensen, S., Søbjaerg, S., Gerland, S., Spreen, G., Bratrein, M., and King, J.: SMOSice 2014: Data acquisition report, Tech. rep., https://earth.esa.int/web/guest/campaignsProject: Technicalsupportforthe2014SMOSicecampaigninSESvalbardESAcontractnumber:4000110477/14/NL/FF/lftechnicalreportNo.1,2014, 2014.

Huntemann, M., Heygster, G., Kaleschke, L., Krumpen, T., Mäkynen, M., and Drusch, M.: Empirical sea ice thickness retrieval during the freeze-up period from SMOS high incident angle observations, Cryosphere, 8, 439–451, https://doi.org/10.5194/tc-8-439-2014, 2014.

Kaleschke, L., Tian-Kunze, X., Maaß, N., Beitsch, A., Wernecke, A., Miernecki, M., Müller, G., Fock, B. H., Gierisch, A. M. U., Schlünzen, K. H., Pohlmann, T., Dobrynin, M., Hendricks, S., Asseng, J., Gerdes, R., Jochmann, P., Reimer, N., Holfort, J., Melsheimer, C., Heygster, G., Spreen, G., Gerland, S., King, J., Skou, N., Søbjærg, S. S., Haas, C., Richter, F., and Casal, T.: SMOS sea ice product: Operational application and validation in the Barents Sea marginal ice zone, Remote Sensing of Environment, 180, 264–273, https://doi.org/http://doi.org/10.1016/j.rse.2016.03.009, 2016.

Ketchum, R.: Airborne laser profiling of the arctic pack ice, Remote Sensing of Environment, 2, 41–52, 1971.

Klein, L. and Swift, C.: An improved model for the dielectric constant of sea water at microwave frequencies, IEEE Transactions on Antennas and Propagation, 25, 104–111, https://doi.org/10.1109/TAP.1977.1141539, 1977.

Landy, J., Isleifson, D., Komarov, A., and Barber, D.: Parameterization of Centimeter-Scale Sea Ice Surface Roughness Using Terrestrial LiDAR, Geoscience and Remote Sensing, IEEE Transactions on, 53, 1271–1286, https://doi.org/10.1109/TGRS.2014.2336833, 2015.

Lawrence, H., Demontoux, F., Wigneron, J. P., Paillou, P., Wu, T. D., and Kerr, Y. H.: Evaluation of a Numerical Modeling Approach Based on the Finite-Element Method for Calculating the Rough Surface Scattering and Emission of a Soil Layer, IEEE Geoscience and Remote Sensing Letters, 8, 953–957, https://doi.org/10.1109/LGRS.2011.2131633, 2011.

Lawrence, H., Wigneron, J. ., Demontoux, F., Mialon, A., and Kerr, Y. H.: Evaluating the semiempirical H-Q model used to calculate the L-band emissivity of a rough bare soil, IEEE Transactions on Geoscience and Remote Sensing, 51, 4075–4084, https://doi.org/10.1109/TGRS.2012.2226995, 2013.

Liu, C., Chao, J., Gu, W., Li, L., and Xu, Y.: On the surface roughness characteristics of the land fast sea-ice in the Bohai Sea, Acta Oceanologica Sinica, 33, 97–106, https://doi.org/10.1007/s13131-014-0509-3, 2014.

Maaß, N., Kaleschke, L., Tian-Kunze, X., and Drusch, M.: Snow thickness retrieval over thick Arctic sea ice using SMOS satellite data, Cryosphere, 7, 1971–1989, https://doi.org/10.5194/tc-7-1971-2013, 2013.

Matzler, C. and Standley, A.: Relief effects for passive microwave remote sensing, International Journal of Remote Sensing, 21, 2403–2412, https://doi.org/10.1080/01431160050030538, 2000.

Mäkynen, M., Cheng, B., and Similä, M.: On the accuracy of thin-ice thickness retrieval using MODIS thermal imagery over Arctic first-year ice, Annals of Glaciology, 54, 87–96, https://doi.org/10.3189/2013AoG62A166, 2013.

Panofsky, H. A. and Brier, G. W.: Some applications of statistics to meteorology, Pennsylvania State University Press, 1958.

Prigent, C. and Abba, P.: Sea surface equivalent brightness temperature at millimeter wavelengths, Annales Geophysicae [0992-7689], 8, 627–634, 1990.

Ricker, R., Hendricks, S., Helm, V., Skourup, H., and Davidson, M.: Sensitivity of CryoSat-2 Arctic sea-ice freeboard and thickness on radar-waveform interpretation, Cryosphere, 8, 1607–1622, https://doi.org/10.5194/tc-8-1607-2014, 2014.

Søbjaerg, S., Kristensen, S., Balling, J., and Skou, N.: The airborne EMIRAD L-band radiometer system, pp. 1900–1903, https://doi.org/10.1109/IGARSS.2013.6723175, 2013.

Stroeve, J. C., Markus, T., Maslanik, J. A., Cavalieri, D. J., Gasiewski, A. J., Heinrichs, J. F., Holmgren, J., Perovich, D. K., and Sturm, M.: Impact of surface roughness on AMSR-E sea ice products, IEEE Transactions on Geoscience and Remote Sensing, 44, 3103–3116, https://doi.org/10.1109/TGRS.2006.880619, 2006.

Strübing, K. and Schwarz, J.: Die Eisverhältnisse in der Barentssee während der IRO-2-Testfahrt mit R/V Lance 17. – 27.03.2014, Tech. rep., abschlussbericht vorgelegt von JS Consulting, Großhansdorf, im Auftrag des AWI, Bestellnummer 12/45086354 zum Werkvertrag Vor -/Nachbereitung und Durchführung der IRO-2-Testfahrt im Rahmen des Vorhabens Entwicklung und Optimierung eines Ozean-Meereis Vorhersagemodells für das Nordpolarmeer, BMWi-Förderkennzeichen: 03SX328H, 2014.

Tian-Kunze, X., Kaleschke, L., Maaß, N., Mäkynen, M., Serra, N., Drusch, M., and Krumpen, T.: SMOS-derived thin sea ice thickness: Algorithm baseline, product specifications and initial verification, Cryosphere, 8, 997–1018, https://doi.org/10.5194/tc-8-997-2014, 2014.

Tiuri, M. E., Sihvola, A. H., Nyfors, E. G., and Hallikaiken, M. T.: The Complex Dielectric Constant of Snow at Microwave Frequencies, IEEE Journal of Oceanic Engineering, 9, 377–382, https://doi.org/10.1109/JOE.1984.1145645, 1984.

Ulaby, F. T. and Long, D. G., Blackwell, W. J., Elachi, C., Fung, A. K., Ruf, C., Sarabandi, K., Zebker, H. A., and Van Zyl, J.: Microwave radar and radiometric remote sensing, University of Michigan Press Ann Arbor, 2014.

Untersteiner, N.: On the mass and heat budget of arctic sea ice, Archiv für Meteorologie, Geophysik und Bioklimatologie Serie A, 12, 151–182, 1961.

Vant, M. R., Ramseier, R. O., and Makios, V.: The complex-dielectric constant of sea ice at frequencies in the range 0.1-40 GHz, Journal of Applied Physics, 49, 1264–1280, 1978.

Warren, S. G., Rigor, I. G., Untersteiner, N., Radionov, V. F., Bryazgin, N. N., Aleksandrov, Y. I., and Colony, R.: Snow depth on Arctic sea ice, Journal of Climate, 12, 1814–1829, https://doi.org/10.1175/1520-0442(1999)012<1814:SDOASI>2.0.CO;2, 1999.

Yu, Y. and Rothrock, D. A.: Thin ice thickness from satellite thermal imagery, Journal of Geophysical Research C: Oceans, 101, 25 753–25 766, https://doi.org/10.1029/96JC02242, 1996.